PTEP

Prog. Theor. Exp. Phys. **2024** 053E01 (26 pages)
DOI: 10.1093/ptep/ptae045

A Superconducting Tensor Detector for Mid-Frequency Gravitational Waves: Its Multichannel Nature and Main Astrophysical Targets

Yeong-Bok Bae [1,2,†], Chan Park [2,3,†], Edwin J. Son [4,†], Sang-Hyeon Ahn[5], Minjoong Jeong[6], Gungwon Kang [1], Chunglee Kim [7], Dong Lak Kim[8], Jaewan Kim [9], Whansun Kim[4], Hyung Mok Lee [3], Yong-Ho Lee [10], Ronald S. Norton[11], John J. Oh [4], Sang Hoon Oh [4], and Ho Jung Paik [11]

[1] *Department of Physics, Chung-Ang University, 84 Heukseok-ro, Dongjak-gu, Seoul 06974, Korea*
[2] *Particle Theory and Cosmology Group, Center for Theoretical Physics of the Universe, Institute for Basic Science (IBS), 55 Expo-ro, Yuseong-gu, Daejeon 34126, Korea*
[3] *Astronomy Research Center, Research Institute for Basic Sciences, Seoul National University, 1 Gwanak-ro, Gwanak-gu, Seoul 08826, Korea*
[4] *National Institute for Mathematical Sciences, 70 Yuseong-daero 1689 beon-gil, Yuseong-gu, Daejeon 34047, Korea*
[5] *Korea Astronomy and Space Science Institute, 776 Daedeok-daero, Yuseong-gu, Daejeon 34055, Korea*
[6] *Supercomputing Center, Korea Institute of Science and Technology Information, 245 Daehak-ro, Yuseong-gu, Daejeon 34141, Korea*
[7] *Department of Physics, Ewha Womans University, 52 Ewhayeodae-gil, Seodaemun-gu, Seoul 03760, Korea*
[8] *Korea Basic Science Institute, 169-148 Gwahak-ro, Yuseong-gu, Daejeon 34133, Korea*
[9] *Department of Physics, Myongji University, 116 Myongji-ro, Cheoin-gu, Yongin 17058, Korea*
[10] *Korea Research Institute of Standards and Science, 267 Gajeong-ro, Yuseong-gu, Daejeon 34113, Korea*
[11] *Department of Physics, University of Maryland, College Park, MD 20742, USA*
*Email: gwkang@cau.ac.kr (G.K.); chunglee.kim@ewha.ac.kr (C.K.)
†These authors contributed equally to this work.

Received November 30, 2023; Revised March 22, 2024; Accepted April 1, 2024; Published April 2, 2024

Mid-frequency band gravitational-wave detectors will be complementary to the existing Earth-based detectors (sensitive above 10 Hz or so) and the future space-based detectors such as the Laser Interferometer Space Antenna (LISA), which will be sensitive below around 10 mHz. A ground-based superconducting omnidirectional gravitational radiation observatory (SOGRO) has recently been proposed along with several design variations for the frequency band of 0.1–10 Hz. For two conceptual designs of SOGRO (i.e. SOGRO and advanced SOGRO [aSOGRO]), we examine their multichannel natures, sensitivities, and science cases. One of the key characteristics of the SOGRO concept is its six detection channels. The response functions of each channel are calculated for all possible gravitational wave (GW) polarizations including scalar and vector modes. Combining these response functions, we also confirm the omnidirectional nature of SOGRO. Hence, even a single SOGRO detector will be able to determine the position of a source and polarizations of GWs, if detected. Taking into account SOGRO's sensitivity and technical requirements, two main targets are most plausible: GWs from compact binaries and stochastic backgrounds. Based on assumptions we consider in this work, detection rates for intermediate-mass binary black holes (in the mass range of hundreds up to $10^5\,M_\odot$) are expected to be 0.0065–8.1 yr^{-1}. In order to detect the stochastic GW background, multiple detectors

© The Author(s) 2024. Published by Oxford University Press on behalf of the Physical Society of Japan. This is an Open Access article distributed under the terms of the Creative Commons Attribution License (https://creativecommons.org/licenses/by/4.0/), which permits unrestricted reuse, distribution, and reproduction in any medium, provided the original work is properly cited.

Downloaded from https://academic.oup.com/ptep/article/2024/5/053E01/7639407 by Ewha Womans University user on 31 October 2024

are required. Two aSOGRO detector networks may be able to put limits on the stochastic background beyond the indirect limit from cosmological observations.

Subject Index E02, F30

1. Introduction

Since the detection of GW150914 [1], the gravitational wave (GW) frequency band between 20 and 2000 Hz has been shown to be fruitful in searching for coalescence of compact binaries composed of stellar-mass black holes (BHs) or neutron stars (NSs). Observations of about 90 such GW events up to the third observing run have been done, opening up a totally new way of exploring the universe. All ground-based laser interferometers such as the advanced Laser Interferometer Gravitational-wave Observatory (aLIGO) [2], advanced Virgo [3], and KAGRA [4] are optimized in this frequency bandwidth.

To broaden the frequency bandwidth, several efforts are underway. These include the Pulsar Timing Arrays (PTAs) [5–9] in the nanohertz GW frequency band, the Laser Interferometer Space Antenna (LISA) in the $10^{-5} - 10^{-1}$ Hz range [10], and the Einstein Telescope (ET) [11] underground that reaches down to 1 Hz. Different frequency bands are targeted to search for different types of GW sources.

Within the past decade, the mid-frequency band between 0.1 and 10 Hz has increasingly drawn attention in the GW community [12]. As we expand the detection frequency down to 0.1 Hz, both the signal-to-noise and the signal duration are expected to be increased for the same source mass. More importantly, this range makes it possible to search for more massive compact binary coalescences in 0.1–10 Hz such as intermediate-mass black hole (IMBH) binary mergers, in addition to providing early warning for stellar-mass binary merger signals. A number of detector concepts for this mid-frequency band have been proposed. They include Superconducting Omnidirectional Gravitational Radiation Observatory (SOGRO) [13,14], DECIhertz interferometer Gravitational-wave Observatory (DECIGO) [15], TOrsion-Bar Antenna (TOBA) [16], Matter wave-laser based Interferometer Gravitation Antenna (MIGA) [17], and Big Bang Observer (BBO) [18].

In particular, the SOGRO concept is unique; it has maximally six detection channels measuring all components of metric perturbations, which in principle enables more efficient removal of the so-called Newtonian gravity noise (NN) that is one of the main technical challenges in the mid-frequencies [19]. The multichannel detection of a single SOGRO detector in principle makes it possible to localize a GW signal.

A tunable "free-mass" GW detector, a predecessor of SOGRO with a single axis, was first proposed with a resonant L-C circuit [20], and a wide-band resonant-mass GW detector was proposed with a resonant lever [21]. To improve the sensitivity, the quantum-limited superconducting quantum interference device (SQUID) [22] and the inductance-bridge transducer [23] were introduced. Then, a superconducting gravity gradiometer (SGG), a miniaturized GW detector with three axes, was developed for sensitive gravity measurements [24] and it became the most sensitive gravity gradient sensor [25,26]. The original concept of SOGRO, which is essentially a large-scale version of this SGG, was proposed in Ref. [13]. Most bar-type GW detectors use the resonant amplification of a bar material responding to passing GWs, and techniques of measuring signals have evolved to using nearly quantum-limited SQUIDs at extremely low temperatures. Interferometer-type detectors, on the other hand, use freely moving test masses

Downloaded from https://academic.oup.com/ptep/article/2024/5/053E01/7639407 by Ewha Womans University user on 31 October 2024

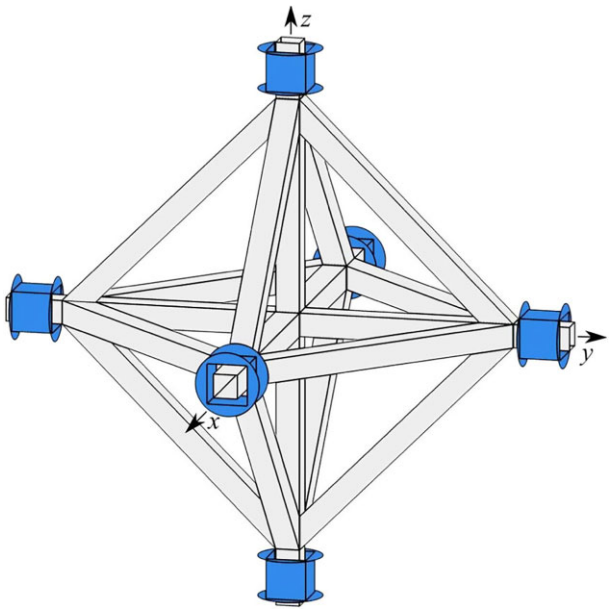


Fig. 1. Perspective view of SOGRO. Motions of six levitated superconducting TMs are combined to measure all six components of the GW strain tensor.

(TMs) whose "elative" motions are measured by the interference of laser lights. SOGRO also uses freely moving TMs, but its relative motions are measured by SQUID devices mounted on a rigid platform at a cryogenic temperature.

Several SOGRO designs have appeared since then. The SOGRO proposed in 2016 [13] has a 30 m arm length of the platform at $T = 1.5$ K. The possibility of constructing a higher-sensitivity SOGRO has been considered by increasing the arm length to 50 m and cooling the antenna to lower temperatures: SOGRO at $T = 4.2$ K and advanced SOGRO (aSOGRO) at $T = 0.1$ K [27]. Even a 100 m arm length was considered in Ref. [14]. Previous works presented detailed specifications of various SOGRO concepts. However, studies on data analysis and target science for the proposed SOGRO detectors remain limited. In this work, therefore, we investigate those aspects applied to two different designs, i.e. SOGRO and aSOGRO, in detail.

In Sect. 3, various properties of the SOGRO in data analysis have been investigated, focusing on the tensorial nature. It includes the response of each channel to GWs, source localization as a single detector, and features of detecting stochastic GW backgrounds. In Sect. 4, the target science of SOGRO has been studied. Detection rates of binary black hole (BBH) mergers and correlations for stochastic GW background are estimated for sensitivities of various SOGRO designs. Finally, we give conclusions with a brief discussion in Sect. 5.

2. Overview of SOGRO

Figure 1 shows a perspective view of SOGRO. Six TMs are levitated at both ends of three orthogonal arms and move freely in any direction. The differential modes of TMs read all six components of the GW strain tensor, which implies the omnidirectional nature of SOGRO, and their common modes (CMs) are rejected by superconducting circuitry [13]. In more detail, in the SOGRO frequency band with 0.1–10 Hz, the wavelengths of GWs are (3–300) $\times$ 10^4 km. Since the distance between TMs is less than 100 m, the wave can be regarded as being

Downloaded from https://academic.oup.com/ptep/article/2024/5/053E01/7639407 by Ewha Womans University user on 31 October 2024

uniform over the detector, e.g. $L/\lambda_{\rm GW} \leq 10^{-5} \leq 1$. Then, in the laboratory frame, the coordinate position of a TM does not move under GWs, but the proper lengths among TMs vary in time. The diagonal component of the wave h_{xx}, for instance, causes oscillation of the proper length between two TMs located on the x-axis, namely, at $+x$ and $-x$, respectively. The off-diagonal component h_{xy}, on the other hand, causes a scissor-like rotational oscillation of four TMs on the xy coordinate plane. Such physical motions of TMs can be combined together to measure GWs as follows [13]:

$$h_{ii}(t) = \frac{2}{L}\left[x_{+ii}(t) - x_{-ii}(t)\right], \tag{1}$$

$$h_{ij}(t) = \frac{1}{L}\left\{\left[x_{+ij}(t) - x_{-ij}(t)\right] - \left[x_{-ji}(t) - x_{+ji}(t)\right]\right\}, \quad i \neq j. \tag{2}$$

Here h_{ij} is the GW strain tensor, L the separation of two TMs on each axis in the absence of GWs, and $x_{\pm ij}(t)$ denotes displacement of the TM on the $\pm i$-axis along the j-axis measured in the so-called Locally Lorentz (LL) frame at the center of the platform.

We note that CM motions of two TMs along each coordinate axis are subtracted out, resulting in no effect on measuring the diagonal component of the wave. Only the differential motions along each coordinate axis can be measured in the diagonal channels. This feature makes the detector very insensitive to seismic noise causing CM linear motion along the axis because sensors mounted on the rigid axis feel such noise as a CM motion of the two TMs. Similarly, differencing between two pairs of TMs in the off-diagonal channel rejects seismic noise causing rotational CM motion of four TMs on the corresponding coordinate plane.

In SOGRO, the tiny motion of TMs induces an electrical signal which is measured by a nearly quantum-limited SQUID amplifier. To avoid the $1/f$ noise appearing in such dc SQUIDs below several kHz, a superconducting capacitor bridge transducer [28] is proposed to be employed in Ref. [13]. This capacitance bridge is driven at pump frequency f_p well above the $1/f$ noise corner frequency of the SQUID. Then the output signal comes out at two sidebands $f_p \pm f$ with the GW frequency $f \ll f_p$.

The detector noise power spectral density (PSD) of the h_{xy} channel of SOGRO was shown [13] to be

$$S_{h,xy}(f) = \frac{16}{ML^2\omega^4}\left[\frac{k_B T \omega_D}{Q_D} + \frac{|\omega^2 - \omega_D^2|}{\omega_p}\left(1 + \frac{1}{\beta^2}\right)^{1/2} k_B T_N\right], \tag{3}$$

where M and L are the mass of each TM and the arm-length of the detector, respectively; T is the temperature; ω_D and Q_D are the differential-mode (DM) (angular) resonance frequency and Q, respectively; and β and T_N are the energy coupling constant of the transducer and the noise temperature of the SQUID, respectively. The energy coupling constant β is given by

$$\beta = \frac{2CE_p^2 Q_p}{M|\omega^2 - \omega_D^2|}\frac{1}{\sqrt{1 + (2Q_p\omega/\omega_p)^2}}, \tag{4}$$

where C is the equilibrium value of each sensing capacitor, E_p is the amplitude of the driving electric field at ω_p, and Q_p is the electrical Q of the transducer. The detector noise PSD of the h_{xx} and h_{yy} channels is twice that given by Eq. (3) due to the fact that displacements of only two TMs are combined to produce those channels, as opposed to the h_{xy} channel for which displacements of four TMs are combined [14].

The design values for detector parameters and the expected detector noise for SOGRO and aSOGRO are given in Table 1 [14]. Both SOGRO and aSOGRO are constructed with TMs of

Downloaded from https://academic.oup.com/ptep/article/2024/5/053E01/7639407 by Ewha Womans University user on 31 October 2024

Table 1. Design parameters for SOGRO detector concepts.

Parameter	SOGRO	aSOGRO	Main feature
Individual TM M (kg)	5000	5000	Multiple-layer Nb shell
Arm length L (m)	50	50	Rigid platform
Antenna temperature T (K)	4.2	0.1	LHe/He^3–He^4 dilution refrigerator
Platform temperature $T_{\rm pl}$ (K)	4.2	4.2	Large cryogenic chamber and cooling system
Platform quality factor $Q_{\rm pl}$	10^5	10^6	Al platform structure
DM frequency $f_{\rm D}$ (Hz)	0.01	0.01	Magnetic levitation (horizontal only)
DM quality factor $Q_{\rm D}$	10^7	10^8	Surface polished pure Nb
Pump frequency $f_{\rm p}$ (kHz)	50	50	Tuned capacitor bridge transducer
Amplifier noise no. n	20	5	Two-stage dc SQUID cooled to 0.1 K
Detector noise $S^{1/2}_{{\rm h},xy}(f)$ ($\rm Hz^{-1/2}$)	1.9×10^{-20}	4.2×10^{-21}	Evaluated at 1 Hz

$M = 5$ tons and with an arm length of $L = 50$ m. For SOGRO, the antenna and the platform are cooled to 4.2 K, and a DM quality factor of 10^7 and a SQUID noise of $20\hbar$ are assumed. For aSOGRO, the antenna is cooled to 0.1 K, and a DM quality factor of 10^8 and a SQUID noise of $5\hbar$ are assumed. The resulting detector noise $S^{1/2}_{h,xy}(f)$ at $f = 1$ Hz is 1.9×10^{-20} $\rm Hz^{-1/2}$ and 4.2×10^{-21} $\rm Hz^{-1/2}$ for SOGRO and aSOGRO, respectively.

In addition to the intrinsic detector noise, the platform thermal noise could also limit the SOGRO sensitivity. To estimate the platform thermal noise for each tensor channel, the thermal displacement noise PSD for each mode was computed and then summed over hundreds of modes that couple to that particular tensor channel [14]. We will discuss how the platform thermal noise affects the sensitivity of SOGRO and aSOGRO in Sect. 4.

3. Tensorial nature of SOGRO

In the previous work, a two-channel GW antenna was studied in a cylindrical shape [29]. It has been extended to an omnidirectional GW antenna in a spherical shape [30,31]. Recently, TOBA has been extended from its original design of a single-channel detector [16] to have three channels to measure three off-diagonal components of the strain tensor in the detector frame [32]. It has been shown that these additional channels can improve GW detection and parameter estimation. SOGRO uses six detection channels, similar to the spherical antenna that uses five channels; thus it is an omnidirectional detector, capable of measuring GWs from any direction. The five channels of the spherical antenna are the combinations of the spherical harmonics, whereas the six channels of SOGRO are the six components of the strain tensor. These two types of omnidirectional detectors are complementary to each other in the sense that the frequency band of SOGRO is mid-frequency, 0.1–10 Hz, and that of the spherical antenna is high frequency, $\gtrsim 2$ kHz.

Note that combining two diagonal channels, e.g. xx and yy channels, gives a LIGO-like interferometer detection channel. Thus, SOGRO is equivalent to a set of six small-size interferometers at the same place, three along the coordinate axes and the other three along the axes 45 degrees rotated about the coordinate axes. In addition, scalar polarizations such as breathing and longitudinal modes of GWs, which may appear in alternative gravity theories, can be measured directly by using diagonal channels. (See Ref. [33] for more details.)

As pointed out in Ref. [14], however, a terrestrial SOGRO is affected by Earth's gravity. As vertical motions of TMs are restricted by the Earth's gravity, the sensitivity for the zz-component of SOGRO is expected to be very poor. This results in only five components of the GW strain

Downloaded from https://academic.oup.com/ptep/article/2024/5/053E01/7639407 by Ewha Womans University user on 31 October 2024

tensor being observable by SOGRO. Thus, these five components will be obtained only from horizontal motions of TMs.

SOGRO is capable of localizing a source as a single detector. Because SOGRO can measure each component of the GW strain tensor separately, it has practically several nonidentical GW channels. The data then can be used to find the direction toward the source. In this section, to see the omnidirectional and tensorial nature of SOGRO, we calculate the response function of a terrestrial SOGRO and briefly show the feasibility of source positioning. Then, the representative sensitivity of a multichannel GW detector is suggested and the noise correlation between channels is considered to estimate the minimum measurable stochastic GW background with a single and multiple SOGRO detectors.

3.1. *Response function*

The tensorial data obtained by a terrestrial SOGRO are of the form

$$s_{ij}(t) = h_{ij}(t) + n_{ij}(t), \tag{5}$$

where n_{ij} is the noise. The observed data s_{ij} and noise n_{ij} are assumed to be symmetric as the strain tensor is.[1] Note that we will not consider s_{33} in the analysis due to the gravity bias. The strain tensor in Eq. (5) is simply written as $h_{ij}(t) = h_{ij}(t, \vec{x} = 0)$ at the location of the detector, $\vec{x} = 0$. The strain tensor can be written as

$$h_{ij}(t, \vec{x}) = \sum_{A=+,\times} e^A_{ij}(\hat{n}) h_A(t - \hat{n} \cdot \vec{x}/c), \tag{6}$$

where $\hat{n}$ is the direction of propagation and h_A the plus- and cross-polarized GW modes. The polarization tensors e^A_{ij} are given by

$$e^+_{ij} = \hat{u}_i \hat{u}_j - \hat{v}_i \hat{v}_j, \qquad e^\times_{ij} = \hat{u}_i \hat{v}_j + \hat{v}_i \hat{u}_j, \tag{7}$$

where two unit vectors $\hat{u}$ and $\hat{v}$ are orthogonal to $\hat{n}$ and to each other. These three unit vectors are explicitly given in terms of the polar and azimuthal angles (θ, ϕ) of the propagating direction $\hat{n}$, respectively, and the polarization angle ψ as in Eq. (A1) in the Appendix. We choose the polarization angle $\psi = 0$ for convenience in what follows unless it is explicitly written. Note that, in this convention, the direction of $\hat{u}$ with respect to which the polarizations are defined is determined once the propagation direction $\hat{n}$ is given, as the intersection between the perpendicular plane to $\hat{n}$ and the x-y plane at a detector.

Recall that the laser interferometer observes scalar data $s(t) = D^{ij} h_{ij}(t) + n(t)$ with $D^{ij} = \frac{1}{2}\left(\hat{x}^i \hat{x}^j - \hat{y}^i \hat{y}^j\right)$, where $(\hat{x}, \hat{y}, \hat{z}) = R_z(-\psi) R_x(\theta) R_z(\pi/2 - \phi)\,(\hat{u}, \hat{v}, \hat{n})$ are the basis vectors in the detector frame and the two arms of the laser interferometer are located in the directions of the x and y axes. Then, the response of the laser interferometer is given by $F_A = D^{ij} e^A_{ij} = \frac{1}{2}\left(e^A_{11} - e^A_{22}\right)$ for the polarization A. Explicitly, the full response functions are given by:[2]

[1] If the observatory observes asymmetric data, then we can use a symmetrized version of Eq. (5), $s_{(ij)}(t) = h_{ij}(t) + n_{(ij)}(t)$, where $x_{(ij)} = \frac{1}{2}(x_{ij} + x_{ji})$ with $x = s, n$.

[2] At first sight, these formulae look slightly different from those in the literature; e.g. they are different from those in Refs. [33,34] in the overall sign. In addition, those in Refs. [35,36] agree with $(-\mathrm{F}_+)$ and $\mathrm{F}_\times$ in this paper (equivalently, F_+ and $(-\mathrm{F}_\times)$ in Refs. [33,34]). These mismatches come from the differences in the coordinate system in the source frame, and all the formulae in this paper and the literature agree with each other up to some rotations. For example, we use the z-x-z rotation to obtain the coordinate system in the source frame, whereas the z-y-z rotation is used in Ref. [33]. The z-x-z rotation is used in Ref. [34] but $\hat{n}$ is rotated by $(-\pi/2)$ with respect to the z-axis, and so on.

Downloaded from https://academic.oup.com/ptep/article/2024/5/053E01/7639407 by Ewha Womans University user on 31 October 2024

$$\mathrm{F}_{+}(\theta,\phi,\psi)=-\frac{1}{2}\left(1+\cos^2\theta\right)\cos 2\phi\cos 2\psi+\cos\theta\sin 2\phi\sin 2\psi, \tag{8}$$

$$\mathrm{F}_{\times}(\theta,\phi,\psi)=\frac{1}{2}\left(1+\cos^2\theta\right)\cos 2\phi\sin 2\psi+\cos\theta\sin 2\phi\cos 2\psi. \tag{9}$$

Then the signal observed at the laser interferometer, ignoring the noise, becomes

$$h(t)=D^{ij}h_{ij}(t)=\mathrm{F}_{+}(\theta,\phi,\psi)h_{+}(t)+\mathrm{F}_{\times}(\theta,\phi,\psi)h_{\times}(t). \tag{10}$$

Note that the polarization angle can be set to be $\psi=0$ without loss of generality. In order to fully determine the four unknowns (i.e. two direction angles and two polarization amplitudes of the GW), therefore, one needs at least three different interferometers from which three outputs $h(t)$ and two independent time delays can be obtained.

Since a SOGRO observes tensorial data (5), the response of each component of the data is simply given by $|e^A_{ij}|$ for polarization A and the total response of a SOGRO is obtained as a quadrature sum of the responses from each component. The response of a SOGRO is depicted in Table 2. The response of the diagonal components—h_{11} and h_{22}—is the same as the response of the cylindrical bar detector up to some rotations. Note that the SOGRO has multiple detection channels. Thus, the signal data measured at each detection channel can be written as

$$h_C(t)=D^{ij}_C h_{ij}(t)=\sum_A D^{ij}_C e^A_{ij}h_A(t)=\sum_A \mathrm{F}^C_A(\theta,\phi,\psi)h_A(t). \tag{11}$$

Here D^{ij}_C are the detector tensors for the detection channels $C=$ (11), (22), (12), (23), (31), respectively. Namely, the channel $C=$ (11) implies the detection for differential motions of the TMs at the ends of the x-axis of the SOGRO, and so $D^{ij}_{11}=\hat{x}^i\hat{x}^j=\delta^i_1\delta^j_1$. Similarly, $D^{ij}_{22}=\hat{y}^i\hat{y}^j$, $D^{ij}_{12}=\frac{1}{2}\left(\hat{x}^i\hat{y}^j+\hat{y}^i\hat{x}^j\right)$, $D^{ij}_{23}=\frac{1}{2}\left(\hat{y}^i\hat{z}^j+\hat{z}^i\hat{y}^j\right)$, $D^{ij}_{31}=\frac{1}{2}\left(\hat{z}^i\hat{x}^j+\hat{x}^i\hat{z}^j\right)$. Then the response functions $\mathrm{F}^C_A(\theta,\phi,\psi)=D^{ij}_C e^A_{ij}=e^A_C$ become

$$\begin{aligned}\mathrm{F}^C_{+}(\hat{\mathbf{n}};\psi)&=\mathrm{F}^C_{+}(\hat{\mathbf{n}})\cos 2\psi+\mathrm{F}^C_{\times}(\hat{\mathbf{n}})\sin 2\psi,\\ \mathrm{F}^C_{\times}(\hat{\mathbf{n}};\psi)&=-\mathrm{F}^C_{+}(\hat{\mathbf{n}})\sin 2\psi+\mathrm{F}^C_{\times}(\hat{\mathbf{n}})\cos 2\psi.\end{aligned} \tag{12}$$

Here $\mathrm{F}^C_A(\hat{\mathbf{n}})\equiv\mathrm{F}^C_A(\theta,\phi,\psi=0)$ are given by

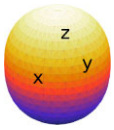
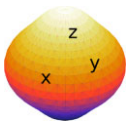
$$\begin{aligned}\mathrm{F}^{(11)}_{+}(\hat{\mathbf{n}})&=1-\left(1+\cos^2\theta\right)\cos^2\phi, \quad \mathrm{F}^{(11)}_{\times}(\hat{\mathbf{n}})=\cos\theta\sin 2\phi,\\ \mathrm{F}^{(22)}_{+}(\hat{\mathbf{n}})&=1-\left(1+\cos^2\theta\right)\sin^2\phi, \quad \mathrm{F}^{(22)}_{\times}(\hat{\mathbf{n}})=-\cos\theta\sin 2\phi,\\ \mathrm{F}^{(12)}_{+}(\hat{\mathbf{n}})&=-\frac{1}{2}\left(1+\cos^2\theta\right)\sin 2\phi, \quad \mathrm{F}^{(12)}_{\times}(\hat{\mathbf{n}})=-\cos\theta\cos 2\phi,\\ \mathrm{F}^{(23)}_{+}(\hat{\mathbf{n}})&=\frac{1}{2}\sin 2\theta\sin\phi, \quad \mathrm{F}^{(23)}_{\times}(\hat{\mathbf{n}})=\sin\theta\cos\phi,\\ \mathrm{F}^{(31)}_{+}(\hat{\mathbf{n}})&=\frac{1}{2}\sin 2\theta\cos\phi, \quad \mathrm{F}^{(31)}_{\times}(\hat{\mathbf{n}})=-\sin\theta\sin\phi.\end{aligned} \tag{13}$$

The magnitudes of some of them are shown in Table 2. Note that F^C_A and h_C can be simply written as $\mathrm{F}^{C=(ij)}_A=e^A_{C=(ij)}=e^A_{ij}$ and $h_{C=(ij)}=h_{ij}$ with the help of the symmetry in e^A_{ij}. The responses of the off-diagonal channels, $\mathrm{F}^{(ij)}_{+,\times}$ with $i\neq j$, are equivalent to those of the three channels of TOBA [32].

Notice that, in principle, a single SOGRO detector can determine all four unknowns because its single measurement with five channels could produce five outputs as in Eq. (11). Note also that the off-axis channel of SOGRO essentially has the same response as LIGO's, e.g. $\mathrm{F}^{(12)}_A(\theta,\phi+\pi/4,\psi)=\mathrm{F}^{\mathrm{LIGO}}_A(\theta,\phi,\psi)$. It follows because the motion of end masses in scissor

Downloaded from https://academic.oup.com/ptep/article/2024/5/053E01/7639407 by Ewha Womans University user on 31 October 2024

Table 2. Responses of each channel in the SOGRO detector for plus (+), cross (×), x, y, breathing (b), and longitudinal (ℓ) polarization modes. The + and × polarizations correspond to tensor modes, the x and y are vector modes, and the b and ℓ polarizations are relevant to scalar modes. The responses of the (22) and the (31) channels are the same as with the (11) and the (23) channels, respectively, up to $\pi/2$ rotation along the z-axis. The (33) channel is not shown as this is not used in sensitivity calculation. Combined (total) responses of all five channels are also depicted. The total responses show the omnidirectional nature of SOGRO; however, the total response of a terrestrial SOGRO to the ℓ mode vanishes in the direction of the z-axis. In the last column, the general responses of a laser interferometer such as LIGO, Virgo, or KAGRA are presented for comparison.

	SOGRO				Interferometer
Modes	(11)	(12)	(23)	total	
+					
×					
unpolarized tensor					
x					
y					
unpolarized vector					
b					
ℓ					

modes is equivalent to the oscillation of mirrors in either the x- or y-arm in the interferometer. Putting this in another way, one can see that the rotation of the laser interferometer by $\pi/4$ with respect to the z-axis yields its detector tensor $D^{ij\prime} = R_z(\pi/4)\frac{1}{2}\left(\hat{x}^i\hat{x}^j - \hat{y}^i\hat{y}^j\right)R_z^{-1}(\pi/4) = \frac{1}{2}\left(\hat{x}^i\hat{y}^j + \hat{y}^i\hat{x}^j\right) = D^{ij}_{(12)}$. Similarly, the SOGRO channels (23) and (32) with appropriate rotations and the combination of SOGRO channels such as $\frac{1}{2}\left(D^{ij}_{(11)} - D^{ij}_{(22)}\right)$ can produce a response identical to that of the laser interferometer. It should be pointed out that these antenna patterns of five detection channels in total make the SOGRO omnidirectional, as can be seen

Downloaded from https://academic.oup.com/ptep/article/2024/5/053E01/7639407 by Ewha Womans University user on 31 October 2024

by the total response function in the column second from the right in Table 2. Namely, at least some of the five channels can measure a nonvanishing signal regardless of the source direction and polarization of a GW. This omnidirectional nature of SOGRO is similar to the spherical resonance detectors such as TIGA and mini-GRAIL [30,31], but SOGRO can cover a much broader frequency band of 0.1–10 Hz.

In alternative gravity theories, in addition to the plus- and cross-polarizations in general relativity, there exist more polarization degrees of freedom such as vector (x and y), breathing (b), and longitudinal (ℓ) polarizations [33,37]. The polarization tensors for the vector and scalar modes are given by $e^x_{ij} = \hat{u}_i\hat{n}_j + \hat{n}_i\hat{u}_j$, $e^y_{ij} = \hat{v}_i\hat{n}_j + \hat{n}_i\hat{v}_j$, $e^b_{ij} = \hat{u}_i\hat{u}_j + \hat{v}_i\hat{v}_j$, and $e^\ell_{ij} = \sqrt{2}\hat{n}_i\hat{n}_j$. The response functions of the laser interferometer for GWs having such polarizations are given by Eqs. (A2) in the Appendix. For SOGRO channels, on the other hand, they are given by Eqs. (A3) in the Appendix. One can easily see that detections by the laser interferometers cannot distinguish the breathing and the longitudinal modes whereas they are not degenerate for the SOGRO detections. In the presence of general polarizations, however, at least two SOGRO detectors at different sites are necessary because we have four more unknowns associated with the amplitudes of four extra polarizations.

3.2. *Combined noise spectral density*

A single SOGRO can be considered as a network of detectors because each channel plays the role of a GW detector, which has its own noise spectral density (NSD). To find a representative NSD of a SOGRO as a single GW antenna, in this section, we try to combine NSDs of channels in a SOGRO.

Firstly, we recall that the optimal matched filter signal-to-noise ratio (SNR) for an interferometer detector such as LIGO, Virgo, or KAGRA is given by

$$\rho^2 = 4\int_0^\infty df\,\frac{\left|\tilde{h}(f)\right|^2}{S_n(f)} = \begin{cases} 2\int_0^\infty df\,\frac{\left|\tilde{h}_+(f)\right|^2+\left|\tilde{h}_\times(f)\right|^2}{S_n(f)}, & \text{(optimal direction)} \\ \frac{4}{5}\int_0^\infty df\,\frac{\left|\tilde{h}_+(f)\right|^2+\left|\tilde{h}_\times(f)\right|^2}{S_n(f)}, & \text{(random direction)} \end{cases} \tag{14}$$

where $S_n(f)$ is the single-sided NSD of the interferometer. The optimal direction in Eq. (14) represents that the GW under consideration is coming from the z-direction (e.g. the vertical direction to the interferometer plane) with a random polarization, where the antenna response of the interferometer becomes maximum. The expected SNR for the optimal direction is calculated by adopting the polarization averaging. The random direction in Eq. (14), on the other hand, represents that the GW is coming from a random direction with a random polarization. Hence, the expected SNR for the random direction is calculated by adopting the total angle averaging. Then, one can define two different versions of the NSD for the interferometer, namely, the *optimal* NSD, S_n, and the *angle-averaged* NSD, $(5/2)S_n$. These NSDs are used to define the sensitivities of the interferometer GW detector.

For the SOGRO detector having multiple channels, if we assume that the noise n_{ij} is stationary Gaussian and each component is uncorrelated with the others, then we have the combined

Downloaded from https://academic.oup.com/ptep/article/2024/5/053E01/7639407 by Ewha Womans University user on 31 October 2024

matched filter SNR [38],

$$\rho^2 = \sum_C \left[4 \int_0^\infty df \, \frac{\left|\tilde{h}_C(f)\right|^2}{S_{n,C}(f)} \right]$$
$$= \sum_C \left[4 \int_0^\infty df \, \frac{F_{+,C}^2 \left|\tilde{h}_+(f)\right|^2 + F_{\times,C}^2 \left|\tilde{h}_\times(f)\right|^2}{S_{n,C}(f)} \right], \tag{15}$$

where $S_{n,\,C}$ is the single-sided NSD of the channel C. Note that, considering GWs with identical waveforms coming in different directions, the combined SNRs in Eq. (15) are not the same in general. It depends on the direction of the GW source. The combined SNR is expected to have its maximal value when a GW is coming from the z-direction, because the maximum response occurs at the z-direction as seen in Table 2.

Now, one can define two kinds of combined NSDs as in the case of the interferometer: one obtained from the maximum SNR and the other from the angle-averaged SNR. Namely, for the maximum SNR, the optimal NSD will be defined as

$$S_n^{(\text{optimal})} = \left[S_{n,(11)}^{-1} + S_{n,(22)}^{-1} + S_{n,(12)}^{-1} \right]^{-1}. \tag{16}$$

This optimal NSD will be used to denote the sensitivities (i.e. $\sqrt{S_n^{(\text{optimal})}}$) for different SOGRO designs in Sect. 4. Next, for the angle-averaged SNR, the angle-averaged NSD is defined as

$$S_n^{(\text{averaged})} = \left[\frac{8}{15} \sum_{C \in \mathcal{D}} S_{n,C}^{-1} + \frac{2}{5} \sum_{C \in \mathcal{D}'} S_{n,C}^{-1} \right]^{-1}, \tag{17}$$

where $\mathcal{D} = \{\text{diagonal channels}\}$ and $\mathcal{D}' = \{\text{off-diagonal channels}\}$. For a terrestrial SOGRO, assuming that $S_{n,\,(11)} = S_{n,\,(22)} \approx 2S_{n,\,(12)} \approx S_{n,\,(23)} = S_{n,\,(31)}$, we have $S_n^{(\text{optimal})} \approx \frac{1}{2} S_{n,(12)} \approx (2/3) S_n^{(\text{averaged})}$.

3.3. *Source localization*

In this section, we show a simple visualization of the source positioning by a single SOGRO. For accurate source localization, we may adopt the localization algorithms for the LIGO–Virgo–KAGRA (LVK) network (see, e.g. Ref. [39] and references therein) because a SOGRO, having multiple channels, can be regarded as a network of detectors. This is out of the scope of the present paper though. Obviously, the triangulation cannot be used for a single SOGRO; however, the response functions of all channels guide us to obtain the position of the source.

Since we observe the tensorial data of Eq. (5), we can find the position of the source even with a single SOGRO. Considering a simulated GW signal propagating in the direction $\hat{n}_0 = (\theta_0, \phi_0)$, the position of the source is in the opposite direction, $-\hat{n}_0$. In order to find $\hat{n}_0$, we first start with the signal h_{ij} without noise for simplicity. Eq. (6) can be rewritten as

$$\begin{bmatrix} h_+ & h_\times & 0 \\ h_\times & -h_+ & 0 \\ 0 & 0 & 0 \end{bmatrix} = R_x(\theta) R_z(\pi/2 - \phi) [h_{ij}] R_z(\phi - \pi/2) R_x(-\theta), \tag{18}$$

where R_k is the rotation matrix with respect to the k-axis. Since h_{ij} is symmetric and traceless and its determinant vanishes, we have four linearly independent equations:

$$h_+ = h_{11} \sin^2\phi - h_{12} \sin(2\phi) + h_{22} \cos^2\phi, \tag{19}$$

Downloaded from https://academic.oup.com/ptep/article/2024/5/053E01/7639407 by Ewha Womans University user on 31 October 2024

$$h_\times = (h_{23}\cos\phi - h_{13}\sin\phi)\sin\theta + \left(\frac{1}{2}(h_{11}-h_{22})\sin(2\phi) - h_{12}\cos(2\phi)\right)\cos\theta, \tag{20}$$

$$\tan\theta = \frac{h_{11}+h_{22}}{h_{13}\cos\phi + h_{23}\sin\phi}, \tag{21}$$

$$\tan 2\phi = \frac{2[h_{12}(h_{11}+h_{22}) + h_{13}h_{23}]}{h_{11}^2 - h_{22}^2 + h_{13}^2 - h_{23}^2}. \tag{22}$$

Given the five measured values of h_{ij} from SOGRO channels, the four unknowns such as θ, ϕ, h_+, and $h_\times$ can be found by solving the four equations above. Note, however, that these four equations are invariant under $\theta \to \pi - \theta$, $\phi \to \phi \pm \pi$, and $h_\times \to -h_\times$. Hence, we cannot distinguish $\hat{n}$ from $-\hat{n}$ in the solution, which is originated from the symmetry of a single SOGRO. To break this degeneracy, we need at least two detectors at separate locations.

By solving Eq. (22), we find four degenerate solutions $\phi = \phi_p + n\pi/2$ in the range of $-\pi < \phi \leq \pi$, where ϕ_p is a particular solution. We then obtain a solution of θ for each ϕ from Eq. (21). Now, h_+ and $h_\times$ are obtained from Eqs. (19) and (20), respectively. Note that, among the four solution pairs, only two satisfy $h_{ij} = \sum_A e_{ij}^A h_A$. The directions given by these two solutions are exactly opposite to each other, $\hat{n}_1 = -\hat{n}_2$; i.e. one is the direction to the source and the other to the GW propagation. Note also that five channels, instead of four, are needed to determine the four unknowns, which was already pointed out in the case of spherical resonant-mass GW detectors [40].

Next, considering noise, a pair of direction vectors, $\hat{n}(t_0)$ and $-\hat{n}(t_0)$, can be obtained at $t = t_0$ by solving Eqs. (19)–(22) with h_{ij} replaced by $s_{ij} = h_{ij} + n_{ij}$. The noise background is expected to shift the solution vectors from the direction of the source, but we can take the average to find the correct direction. As a simple realization, we consider a sine-wave signal, $h_+ = a_+\cos(\omega_0 t)$ and $h_\times = a_\times \sin(\omega_0 t)$, over a Gaussian noise background of distribution $\mathcal{N}(0, \sigma^2)$. The position (θ_0, ϕ_0) of the simulated signal is marked by a star in Fig. 2. The estimated positions are plotted as "×" at every time step. The amplitudes are set $a_+ = a_\times = 1$ and the standard deviation of the noise background is $\sigma = 0$ for Fig. 2(a), $\sigma = 0.1$ (SNR 167.9) for Fig. 2(b), $\sigma = 0.2$ (SNR 83.94) for Fig. 2(c), $\sigma = 0.3$ (SNR 55.96) for Fig. 2(d), $\sigma = 0.4$ (SNR 41.97) for Fig. 2(e), and $\sigma = 0.5$ (SNR 33.57) for Fig. 2(f).

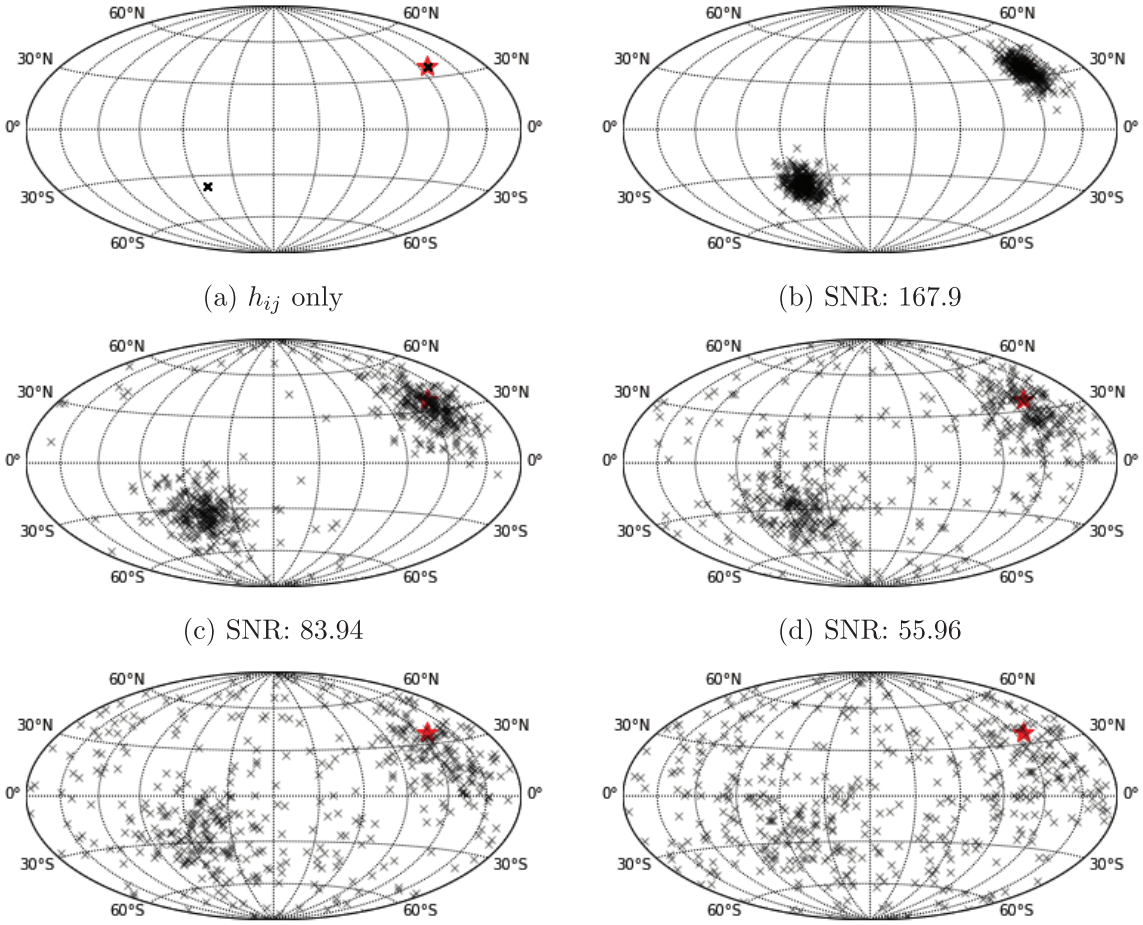
3.4. *Correlation for multidetectors with multichannels*

In this section, we consider the data analysis required for the detection of a stochastic gravitational wave background (SGWB) using SOGRO detectors. In particular, the dimensionless spectral energy density $\Omega_{\rm gw}(f) = (d\rho_{\rm gw}/d\ln f)/\rho_{\rm cr}$ has been analyzed, taking into account the multichannel nature of SOGRO. Recall that the minimum detectable value of $\Omega_{\rm gw}(f)$ in a single interferometer is given by [41]:

$$\left[\Omega_{\rm gw}(f)\right]_{\rm min} = \frac{4\pi}{3H_0^2} f^3 S_n(f) \frac{\rho^2}{F}, \tag{23}$$

where the angular efficiency factor is given by $F = \langle F_+^2\rangle + \langle F_\times^2\rangle = 2/5$ for terrestrial interferometers. $H_0 = h_0 \times 100\,\mathrm{km/s/Mpc}$ is the Hubble constant today. Since the off-diagonal channels in a single SOGRO detector have the same angular efficiency factor, each detection channel gives the same minimum detectable value for $\Omega_{\rm gw}(f)$. One might think of a SOGRO as multiple

Downloaded from https://academic.oup.com/ptep/article/2024/5/053E01/7639407 by Ewha Womans University user on 31 October 2024



(a) h_{ij} only (b) SNR: 167.9

(c) SNR: 83.94 (d) SNR: 55.96

(e) SNR: 41.97 (f) SNR: 33.57

Fig. 2. Localization for a simulated sine-wave signal over a Gaussian noise background. We assume all five channels are working at the design sensitivity. Standard deviations of the noise are assumed to be (a) zero, (b) 1/10 of the amplitude of the signal (SNR 167.9), (c) 1/5 of the amplitude of the signal (SNR 38.94), (d) 3/10 of the amplitude of the signal (SNR 55.96), (e) 2/5 of the amplitude of the signal (SNR 41.97), and (f) 1/2 of the amplitude of the signal (SNR 33.57). The position of the synthetic source signal is marked with a star. The calculated positions at every t are shown as "$\times$." The degeneracy of two *positions* in all panels is expected due to the symmetry of the response function of a single SOGRO.

interferometers at the same location, from which we may have some gain. However, the overlap reduction functions between any two of the off-diagonal channels defined by

$$\Gamma(f) = \int \frac{d^2\hat{n}}{4\pi} \int \frac{d\psi}{2\pi} \left[\sum_A \mathrm{F}_A^{(1)}(\hat{n}) \mathrm{F}_A^{(2)}(\hat{n}) \right] \exp\left(2\pi i f \hat{n} \cdot \Delta\vec{x}/c\right) \tag{24}$$

are vanishing, where $\Delta\vec{x} = \vec{x}_{(2)} - \vec{x}_{(1)} = 0$ for this case. As for the diagonal channels, on the other hand, the angular efficiency factors are given by $F = 8/15$ and the overlap reduction functions between two of three diagonal channels are calculated as $\Gamma = -4/15$. Since we have two independent pairs of the diagonal channels, the minimum value of $\Omega_{\mathrm{gw}}(f)$ in a single SOGRO is given by

Downloaded from https://academic.oup.com/ptep/article/2024/5/053E01/7639407 by Ewha Womans University user on 31 October 2024

$$\left[\Omega_{\rm gw}(f)\right]_{\rm min} \sim \frac{5\pi^2}{H_0^2}\frac{f^3\rho^2}{(2T\Delta f)^{1/2}}\left[S_{n,11}(f)S_{n,22}(f)\right]^{1/2} \tag{25}$$

$$\simeq 8.78\times10^{-3}\left(\frac{0.73}{h_0}\right)^2\left(\frac{f}{1\,\rm Hz}\right)^3\left(\frac{\rho}{5}\right)^2 \times\left(\frac{1\,\rm yr}{T}\frac{10\,\rm Hz}{\Delta f}\right)^{1/2}\left(\frac{S_{n,\rm diag}}{1\times10^{-36}\,\rm Hz^{-1}}\right), \tag{26}$$

where T is the integration time and Δf the frequency band of the detector, assuming that the sensitivity is flat in the band. The NSDs of diagonal channels are assumed to be the same, $S_{n,\,ii} = S_{n,\,\rm diag}$ with $i = 1, 2$. In this derivation, noises of different channels are assumed to be independent, i.e. uncorrelated. The Brownian motion for each channel comes from thermal noise in different combinations of modes and the SQUID noise comes from different SQUIDs. Hence, they are generally uncorrelated. The platform noise may be correlated between some channels. The Newtonian noise coming from seismic or atmospheric density fluctuations in the surround may also give correlation. These correlated noises will not be suppressed by the time integration and so the upper bound of $\Omega_{\rm gw}(f)$ measured by a single SOGRO should be limited by these noises.

We now consider a network of two identical SOGRO detectors which are located at some distance d from each other, but in the same orientation for convenience. We assume that their separation is far enough that the noises of two detectors are uncorrelated, but still close enough that the exponential factor in the overlap reduction function in Eq. (24) approximates to 1. Then, the overlap reduction functions between two detectors simply reduce to 8/15 for the diagonal channels in the same direction, −4/15 for the diagonal channels in the different direction, and 2/5 for the off-diagonal channels in the same direction, respectively. The NSD of the x-y channel is roughly half of the NSDs in other channels, i.e. $S_{n,\,ii} \approx S_{n,\,i3} \approx 2S_{n,\,12}$ with $i = 1, 2$ in SOGRO. For two SOGRO detectors, finally, the minimum detectable value of $\Omega_{\rm gw}(f)$ approximates to

$$\left[\Omega_{\rm gw}(f)\right]_{\rm min} \sim \frac{4\pi^2}{3H_0^2}\frac{f^3\rho^2}{(2T\Delta f)^{1/2}}\left[\frac{32}{45}S_{n,\,\rm diag}^{-2} + \frac{4}{25}\left(S_{n,12}^{-2} + S_{n,23}^{-2} + S_{n,31}^{-2}\right)\right]^{-1/2} \tag{27}$$

$$\simeq 1.81\times10^{-3}\left(\frac{0.73}{h_0}\right)^2\left(\frac{f}{1\,\rm Hz}\right)^3\left(\frac{\rho}{5}\right)^2 \times\left(\frac{1\,\rm yr}{T}\frac{10\,\rm Hz}{\Delta f}\right)^{1/2}\left(\frac{S_{n,\,\rm diag}}{1\times10^{-36}\,\rm Hz^{-1}}\right). \tag{28}$$

As mentioned above, however, the correlation between noises of different channels at the same detector may not be removed completely. Hence, the network of different channels at the same detector has not been taken into account in this formula.

For the SOGRO network of N identical detectors, with the same orientation and the same assumption that they are still close enough to keep the overlap reduction functions unchanged, the minimum detectable value of $\Omega_{\rm gw}(f)$ becomes $\sqrt{2/N(N-1)}$ times Eq. (27). It should be noted here that N is restricted not to be a large number because of the strong assumptions—the same orientation and close locations.

Downloaded from https://academic.oup.com/ptep/article/2024/5/053E01/7639407 by Ewha Womans University user on 31 October 2024

4. Target science of SOGRO

Previous papers on SOGRO [13,14] have primarily focused on detection principles and instrument sensitivity, and have not much discussed the astrophysical targets observable by using SOGRO. In this section, we compare the sensitivities of SOGRO and GW signal expected from IMBH binaries, which are considered to be the main observation targets of SOGRO, and calculate the horizon distances and detection rates. We also discuss the detectability of stochastic GW backgrounds with the SOGRO network, assuming several cosmological and astrophysical models.

4.1. *Coalescence of BBHs*

Since the first detection of GW150914 by aLIGO [1] in 2015, about 90 compact binary coalescences have been observed [42–45]. They include stellar-mass BH–BH, NS–NS, and NS–BH binaries. The detectable mass range for LVK detectors is less than a few hundred solar masses because their most sensitive frequency band is about 20–2000 Hz.

More massive BBHs are the prime target for SOGRO, given its coverage of the frequency band between 0.1 and 10 Hz. The highest GW frequency in the inspiral phase—innermost stable circular orbit (ISCO)—is inversely proportional to the binary's total mass as follows [46]:

$$f_{\mathrm{GW,ISCO}} = \frac{1}{\pi}\left(\frac{1}{6}\right)^{1.5}\frac{c^3}{GM} \sim \frac{4396}{M/M_\odot}\ [\mathrm{Hz}]. \tag{29}$$

Hence, SOGRO can observe only the inspiral phase of compact binaries with masses less than approximately 440 $M_\odot$. Conversely, for binaries with masses exceeding 44,000 $M_\odot$, only the merger and ringdown phases are observable. Even when considering the merger and ringdown phases, the observable mass range with SOGRO is limited up to roughly 10^5 $M_\odot$.

BHs with masses in the range $\sim 10^2$–10^5 $M_\odot$ are termed IMBHs. The mass range of the targeted compact binaries of SOGRO overlaps with that of the IMBHs. The existence of IMBHs can be inferred from the straightforward extrapolation of the well-known correlation between a galaxy bulge's stellar velocity dispersion and the mass of its supermassive BH [47–51]. Although several observations support the existence of IMBHs [52–56], their existence still remains a topic of debate [57].

In this section, we evaluate the detectability of IMBH binaries (IMBHBs) by considering SOGRO's sensitivity and estimate their detection rates based on an assumption of their formation in star clusters. We utilize analytical waveforms encompassing inspiral, merger, and ringdown phases with nonprecessing BH spins [58]. Furthermore, we adopted the cosmological parameters from the Planck mission [59] to compute the distance scale.

Figure 3 displays the sensitivity curves of SOGRO and aSOGRO obtained from Table 1 and Eq. (16), represented by orange dashed and blue solid lines, respectively.[3] Here the plot is the sum of the antenna thermal, amplifier, and platform thermal noises, and the noise models introduced in Ref. [14] are used with the design parameters in Table 1. The platform thermal noise

[3]It should be pointed out that the definition of the detector sensitivity in Eq. (16) differs from that in Ref. [14], which is simply the sum of all five channels. The definition in Ref. [14] is neither the optimal NSD nor the direction-averaged one. Here, the platform quality factors of SOGRO and aSOGRO $Q_{\mathrm{pl}} = 10^6, 10^7$ are used, respectively, for the reason explained in Ref. [14].

Downloaded from https://academic.oup.com/ptep/article/2024/5/053E01/7639407 by Ewha Womans University user on 31 October 2024

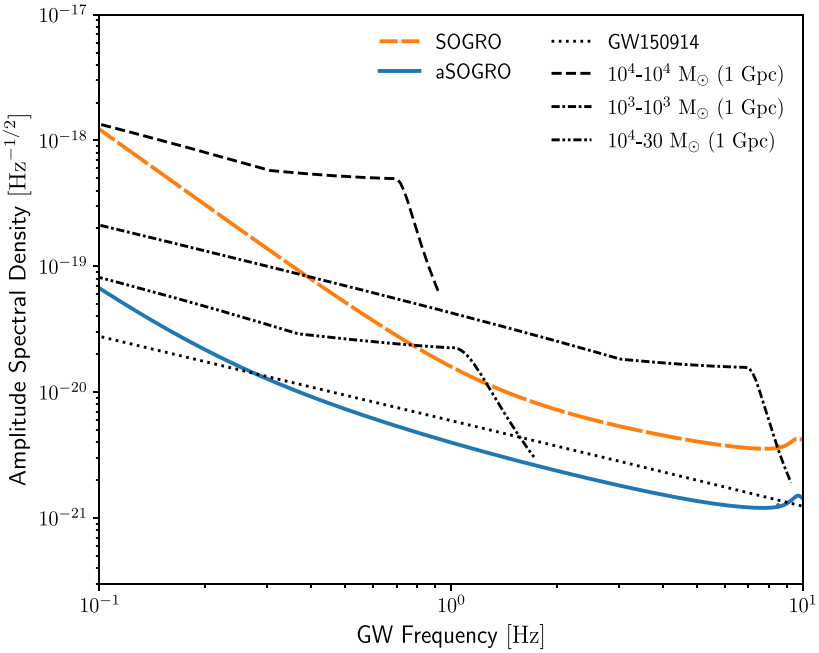


Fig. 3. Combined NSDs (16) of SOGRO and aSOGRO are overlaid with the amplitude spectral densities (ASDs) of the expected signal from BBHs with different masses. The inclinations of BBHs are assumed to be zero (face-on). GW150914 signal is based on its observed masses and distance as given in the literature [42]. For the BBHs with IMBHs, the masses and distances are assumed to be as indicated in the figure.

critically depends on the structural design and Q of the platform. In the tentative design investigated, the amplitude spectral densities (ASDs) of SOGRO and aSOGRO were dominated by the platform thermal noise in the frequency band of 1–10 Hz [14]. The seismic and Newtonian noises are assumed to be suitably mitigated below the sensitivity curves. Black lines denote the ASDs for BBHs with various masses and mass ratios. Given the observed samples, aSOGRO's sensitivity can reach the ASD of GW150914 within its detection frequency band, with a SNR of $\rho \simeq 2.6$. For IMBHs, we simplify the source models by assuming all BBHs are at 1 Gpc. aSOGRO has the capability to detect all IMBHs considered in Fig. 3. SOGRO can also detect a 10^4–10^4 $M_\odot$ and a 10^3–10^3 $M_\odot$ binary at 1 Gpc with $\rho \simeq 10$ and $\rho \simeq 5$, respectively.

Figure 4 illustrates the horizon distances of SOGRO and aSOGRO as functions of the total mass of a BBH. Here, the horizon distance is defined as the maximum observable distance when the BBH is located at the zenith of the SOGRO with zero inclination for a given SNR $\rho = 8$. The overall shape of the horizon distance is determined by the sensitivity curve's shape and the frequency range of GW signals from the BBHs. Since massive BBHs merge before reaching 10 Hz, the horizon distance decreases in the regime of the large total mass. The optimal total mass for detecting BBHs, corresponding to the expected sensitivities, is roughly (2–5) $\times$ 10^4 $M_\odot$ for aSOGRO and about 10^4 $M_\odot$ for SOGRO, respectively, in the case of the equal-mass BBHs. The maximum horizon distances of SOGRO and aSOGRO for equal-mass BBHs are approximately $z \simeq 0.25$ and 0.99, corresponding to a luminosity distance of roughly 1.3 Gpc and 6.7 Gpc, respectively. These values match or surpass the distances of BBHs observed by current interferometric GW detectors. We also calculated the horizon distance of IMBH–IMBH binaries with a mass ratio of 10, and binaries of an IMBH with a 30 $M_\odot$ stellar-mass

Downloaded from https://academic.oup.com/ptep/article/2024/5/053E01/7639407 by Ewha Womans University user on 31 October 2024

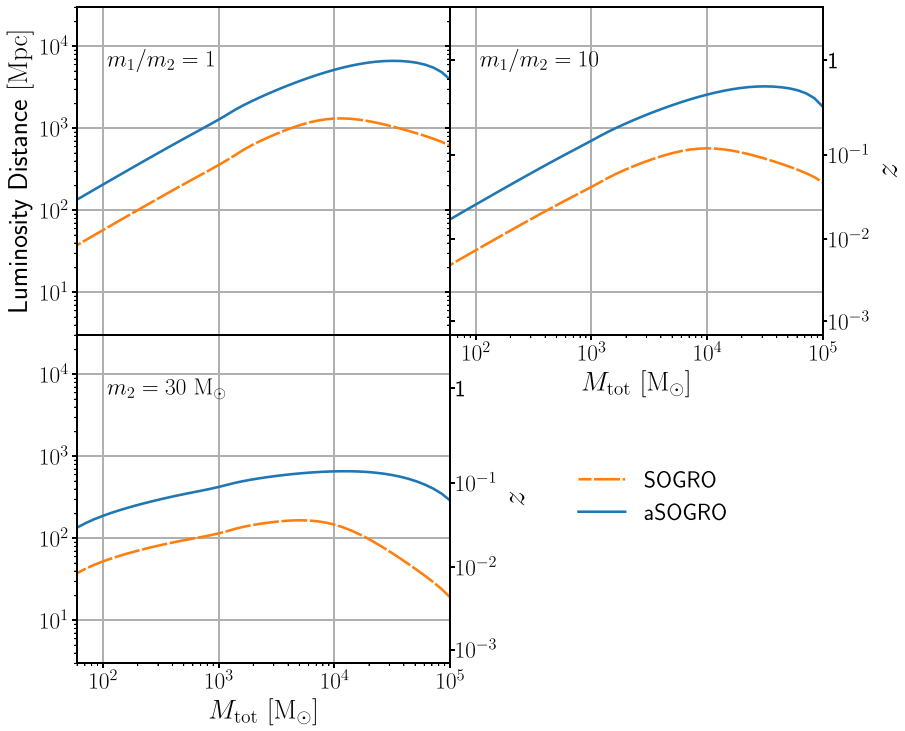


Fig. 4. Horizon distances versus the total mass of BBHs based on the sensitivities of SOGRO (orange dashed lines) and aSOGRO (blue solid lines), respectively. We consider the cases where the mass ratios are $m_1/m_2 = 1$ and 10, and additionally when the secondary mass is fixed to be 30 $\mathrm{M}_\odot$. All BBHs are assumed to be face-on and $\rho = 8$. The redshift z is also designated on the right-hand side.

BH (sBH), which yield smaller horizon distances than equal-mass IMBH–IMBH binaries due to their smaller chirp masses. The horizon distance of aSOGRO for the IMBH–sBH binary extends up to $z \simeq 0.14$. It should be noted that the mass ratio in the IMBH–sBH plot is dependent on the horizontal axis.

To estimate the detection rate of IMBHBs, we must first make assumptions regarding their formation history. While several formation mechanisms have been proposed [60], our understanding of them remains limited. In this study, we adopt the methodology of earlier research [61,62]. These studies postulate that IMBHs originate from the collapse of a very massive star, which itself forms via a runaway collision of massive main-sequence stars in a young dense star cluster [63–67]. In this cluster, two independently formed IMBHs can be gravitationally bound to become a binary, which subsequently merges in a short time.

The overall process of estimating the detection rate is as follows. We use the star formation rate in mass (M_{SF}) per unit comoving volume (V_c) per unit time at the detector (t_0) to find the number of star clusters among which IMBHBs are formed and integrate it up to the detectable volume which is calculated by using angle-averaged sensitivity (17). If we consider the distribution function of the mass of the clusters $\mathrm{f}(M_{\mathrm{cl}})$ in calculating the number of clusters, the detection rate R can be expressed as follows (Eqs. (2) and (4) in Ref. [61]):

$$R = \int_0^{z_{\max}} \frac{d^2 M_{\mathrm{SF}}}{dV_c dt_e} \frac{dt_e}{dt_0} g_{cl} g \int_{M_{\mathrm{cl,min}}(z)}^{M_{\mathrm{cl,max}}(z)} \frac{\mathrm{f}(M_{\mathrm{cl}})}{\int M_{\mathrm{cl}} \mathrm{f}(M_{\mathrm{cl}}) dM_{\mathrm{cl}}} dM_{\mathrm{cl}} \frac{dV_c}{dz} dz\,, \tag{30}$$

Downloaded from https://academic.oup.com/ptep/article/2024/5/053E01/7639407 by Ewha Womans University user on 31 October 2024

Table 3. Estimated detection rates for equal-mass BBH mergers. The most conservative ($R_{\rm low}$), reference ($R_{\rm ref}$), and the most optimistic ($R_{\rm high}$) estimates are presented with the model assumptions. We present the detection rates obtained for two values of the SNR for comparison: $\rho = 8$ (without parentheses) and $\rho = 5$ (within the parentheses). Details of model assumptions can be found in the main text.

	$\rm R_{low}$	$\rm R_{ref}$	$\rm R_{high}$
	$\rho = 8$ (5), equal mass, no spin, randomly oriented source		
Model assumption	$M_{\rm BBH,\,max} = 2 \times 10^4\ \rm M_\odot$ $g_{\rm cl} = 0.0025$ $g = 0.1$ $R_{\rm double}/R_{\rm single} = 0.1$	$M_{\rm BBH,\,max} = 10^5\ \rm M_\odot$ $g_{\rm cl} = 0.01$ $g = 0.2$ $R_{\rm double}/R_{\rm single} = 0.5$	$M_{\rm BBH,\,max} = 10^5\ \rm M_\odot$ $g_{\rm cl} = 0.1$ $g = 0.5$ $R_{\rm double}/R_{\rm single} = 1$
Detection rate ($\rm yr^{-1}$)	0.0065 (0.018)	0.093 (0.24)	3.1 (8.1)

where t_e is the local time at the source, and the parameters $g_{\rm cl}$ and g are the fraction of the mass included in the star cluster and the fraction of the clusters that can produce IMBHBs, respectively.

We use three different models for the star formation rates [68–70] adopted in Ref. [71]. But these models do not give much difference in detection rates (about 10% at most), because their differences are conspicuous out of the horizon distance of aSOGRO. Thus, we use the average value of them. For the fraction parameters that are the most uncertain factors, we consider the conservative and optimistic ranges from the literature as $g_{\rm cl} \sim$ (0.0025–0.1) [61,62,72] and $g \sim$ (0.1–0.5) [61,62,73,74], respectively. In addition, we adopt the distribution function of the mass of the cluster as $\rm f(\mathit{M}_{cl}) \propto \mathit{M}_{cl}^{-2}$ from Ref. [75]. We assume the lowest mass of the IMBHB in the mass distribution to be 200 $\rm M_\odot$ [62], and the mass ratio between the IMBHB and the star cluster to be $M_{\rm BBH}/M_{\rm cl} = 2 \times 10^{-3}$ [67], which means the lower mass limit of the cluster that can have IMBHBs is $10^5\ \rm M_\odot$. The lower limit in the integration of the cluster mass in Eq. (30) is selected as the larger one between $10^5\ \rm M_\odot$ and the minimum cluster mass considering the detector's sensitivity and the distance to the source, since the detectable IMBHB's mass is larger than 200 $\rm M_\odot$ when the source is far away. The upper limit of the integration is also chosen as the smaller one between $10^7\ \rm M_\odot$, which is the upper limit of the cluster mass considered in Ref. [75], and the maximum cluster mass detectable at a given distance. Thus, the IMBHB's mass range used in the calculation of the detection rate is $2 \times 10^2 - 2 \times 10^4\ \rm M_\odot$. But SOGRO can detect the BH binaries with higher mass (Fig. 4), so the same trend of the mass distribution is extended to the larger masses when the reference and optimistic detection rates are estimated.

The above calculation assumes that the IMBHBs are formed in a single star cluster. However, two IMBHs that are formed in different star clusters can merge by the collision of the star clusters. It is known that about 10%–100% of the number of IMBHBs can be added through this double cluster scenario [76]. Thus, the final estimation of the detection rate is presented by multiplying the above calculations by 1.1 and 2 for the conservative and the optimistic estimations, respectively. The estimations of the detection rate of SOGRO are presented in Table 3.

We have categorized the estimated detection rate of aSOGRO into three cases—the most conservative, the most optimistic, and a reference value between them. The conditions for each of these categories are detailed in Table 3. Additionally, we considered cases with

Downloaded from https://academic.oup.com/ptep/article/2024/5/053E01/7639407 by Ewha Womans University user on 31 October 2024

$\rho = 5$, which are indicated in parentheses. In our estimations of the detection rates, we assumed the averaged combined sensitivity of aSOGRO and the random orientation of BBHs.

With aSOGRO, in the most optimistic scenario, we anticipate approximately 3–8 detections per year. However, in the least favorable scenario, the detection of IMBHs becomes nearly infeasible. The most likely detection rates lie between 0.1 and 0.24 per year. As it stands, the sensitivity of aSOGRO may need further enhancement for IMBHB detections. However, it is still premature to make a definitive conclusion due to the significant gap between the conservative and the optimistic estimates, stemming from the limited information on IMBHs.

We can also estimate the detection rate of IMBH–sBH binaries since their GW frequency is dependent on their total mass (see Eq. (29)). However, their horizon distances are significantly shorter than those of IMBH–IMBH binaries because their chirp masses are dominated by the sBH. Considering that the observable volume is proportional to the cube of the horizon distance, this results in a significantly reduced detection rate. Moreover, considering that only about 1% [77] of IMBHs are paired with a sBH, the rate would be even lower. Although the formation scenario wherein IMBHs grow via successive mergers with sBHs could potentially enhance the detection rate [78,79], it remains doubtful that it would lead to a substantial increase in SOGRO's detection rates, because the mass of BBHs in the early growth stages is small, implying a limited observable volume.

SOGRO's frequency band encompasses the inspiral phase of binaries made up of two sBHs or NSs, even though their merger and ringdown phases fall outside of this range. The inspiral signals from these sources linger within SOGRO's frequency band for an extended period. For instance, a 30–30 $M_\odot$ BBH remains in the 0.1–10 Hz range for approximately two weeks, which is equivalent to roughly 10^5 cycles [80]. Detecting such signals would be invaluable for accurately estimating source parameters and testing general relativity [77]. Moreover, it could be beneficial for higher-frequency detectors and electromagnetic follow-ups by providing early warnings. For a randomly oriented equal-mass 30–30 $M_\odot$ BBH considering the averaged combined sensitivity of aSOGRO, the observable comoving volume is approximately 4.3×10^{-3} Gpc^{-3} at $\rho = 5$. Given that the expected BBH merger rate in GWTC-3 is (17.9–44) Gpc^{-3} yr^{-1} [81], the detection rate in aSOGRO can reach up to about 0.2 yr^{-1}. This implies the potential for aSOGRO to play a certain role in the observation of stellar-mass BHs.

We can also explore the GWs emitted from the inspiral phase of subsolar-mass BBHs. They are not formed through stellar evolution. Some theories suggest that early universe density fluctuations might spawn primordial BHs [82], while others hint at production by nonbaryonic dark matter particles [83]. Figure 5 compares the ASD for a 1–1 $M_\odot$ with those of detectors, and depicts the horizon distance of aSOGRO with respect to the total mass of the subsolar-mass BBHs. Due to their small chirp masses, aSOGRO's horizon distance for subsolar BBHs is limited to several Mpc. This corresponds to the size of the Local Group which includes the Milky Way and M31. Constraints from the first half of aLIGO and Virgo's third observing run imply a merging rate of about 1200 Gpc^{-3} yr^{-1} for 1–1 $M_\odot$ subsolar-mass BBHs [84]. Taking into account this merger rate at face value, we anticipate aSOGRO's detection rate for subsolar-mass BBHs to be no more than roughly 2.5×10^{-3} yr^{-1}.

Downloaded from https://academic.oup.com/ptep/article/2024/5/053E01/7639407 by Ewha Womans University user on 31 October 2024

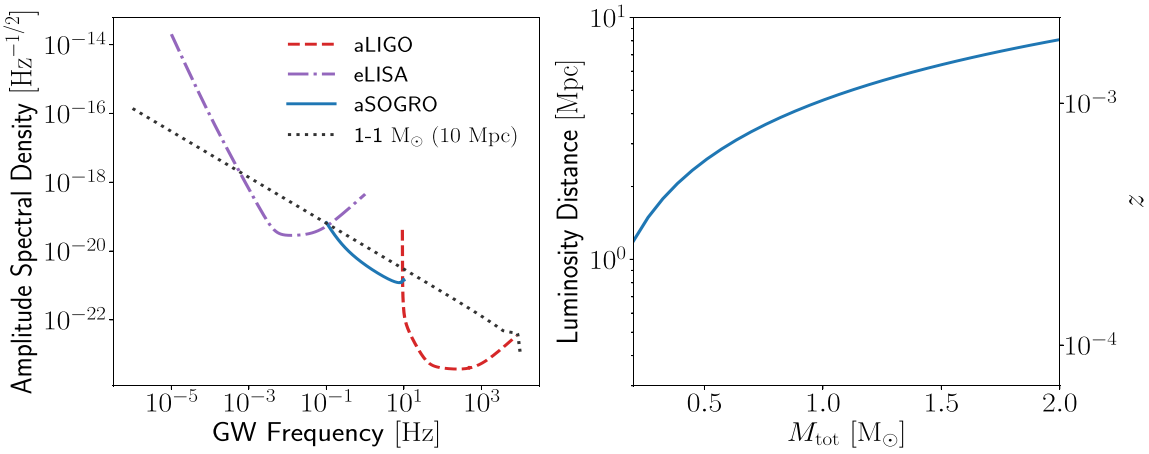


Fig. 5. (Left) Expected GW signal from an equal-mass (1 $M_\odot$) BBH coalescence and the sensitivity curves of aLIGO, eLISA, and aSOGRO. (Right) Horizon distance with respect to the total mass of BBHs when the mass ratio is 1. The curve is based on the fixed SNR $\rho = 8$.

4.2. *Stochastic background*

In the two-detector correlation as in Eq. (27), let us assume the power-law model for SGWB $\Omega_{\rm gw}(f) = \Omega_0(f/f_0)^\alpha$ for real α. Then, the minimum detectable model with SNR ρ is given by

$$\Omega_{\rm gw}^{\rm min}(f) = \frac{4\pi^2}{3H_0^2}\frac{\rho^2}{\sqrt{2T}}\left[\int_0^\infty df' f'^{2(\alpha-3)} S_{n,\rm cor}^{-2}(f')\right]^{-1/2} f^\alpha, \tag{31}$$

where

$$S_{n,\rm cor}(f) = \left[\frac{32}{45}S_{n,\rm diag}^{-2}(f) + \frac{4}{25}\left(S_{n,12}^{-2}(f) + S_{n,23}^{-2}(f) + S_{n,31}^{-2}(f)\right)\right]^{-1/2}. \tag{32}$$

Here, all detections by pairs of channels at the same detector are ignored due to the potential noise correlation among nearby channels. Overlapping the curves of minimum detectable models over a certain range of α, we obtain the power-law integrated (PI) sensitivity curve [85].

Figure 6 shows PI sensitivity curves for several SOGRO types in a frequency range of $0.1\,{\rm Hz} \le f \le 10\,{\rm Hz}$. As possible SGWB candidates near SOGRO's frequency band, we depict rough levels of a cosmological SGWB generated during the inflation era from Ref. [86] and an astrophysical SGWB [87] generated by BBHs and binary neutron stars (BNSs). We also plot the indirect limits [88], which is the upper bound of the SGWB reconciled with the concordance cosmological model. For comparison, we show the sensitivity of LISA [89] in $10^{-4}\,{\rm Hz} \le f \le 1\,{\rm Hz}$ and the PI sensitivity for the 3-detector network consisting of two aLIGOs and Virgo [87], labeled as Design HLV, in $10\,{\rm Hz} \le f \le 130\,{\rm Hz}$. For all PI curves, we use the power range $-10 \le \alpha \le 10$, the observation time interval $T = 2\,{\rm yr}$, the SNR $\rho = \sqrt{2}$, and the Hubble constant $H_0 = 68\,{\rm km/s/Mpc}$. The curve labeled as "Inflation" is the strength of the SGWB from cosmological inflation [86] with the tensor-to-scalar ratio $r = 0.1$ [90]. The curve labeled as "BBH+BNS" is the strength of the astrophysical SGWB from BBHs and BNSs [87]. The curve labeled as "Indirect Limits" shows the upper bound of the SGWB constrained by cosmological observations [88]. SOGRO's frequency band is complementary with other detectors and/or constraints. We expect that LISA, aLIGO, and aSOGRO can explore the SGWB beyond the cosmological indirect limits in their own frequency range.

Downloaded from https://academic.oup.com/ptep/article/2024/5/053E01/7639407 by Ewha Womans University user on 31 October 2024

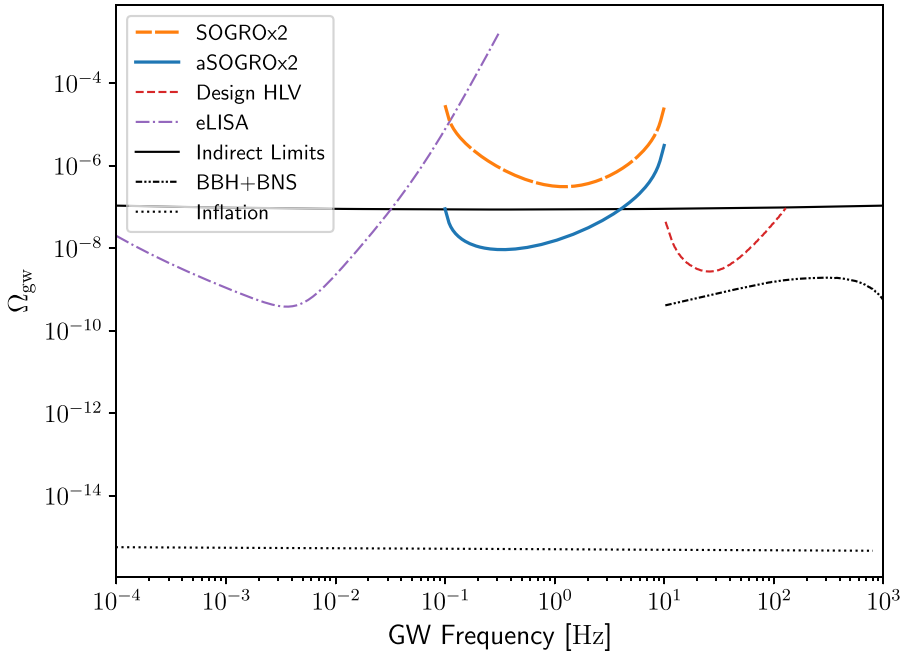


Fig. 6. PI sensitivity curves for different detectors for the SGWB. In addition, theoretical predictions and constraints are shown. The two-detector configurations with SOGRO (orange dashed line) and aSOGRO (blue solid line) are presented in a frequency range of $0.1\,\text{Hz} \leq f \leq 10\,\text{Hz}$.

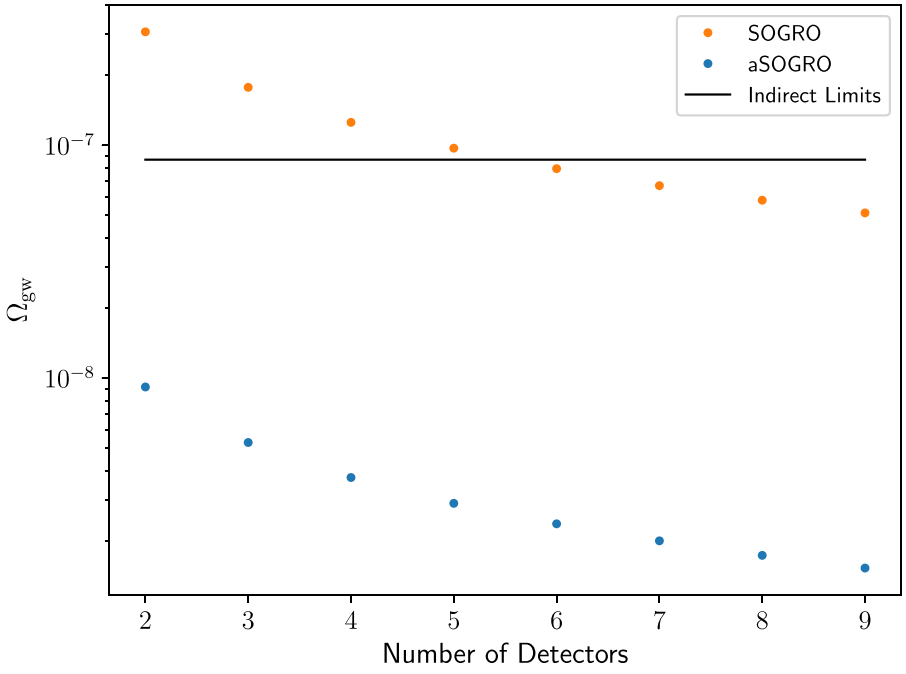


Fig. 7. Expected sensitivities for SGWB observation by considering networks of multiple SOGRO or aSOGRO detectors. The SGWB is assumed to follow the power-law model with $\alpha = 0$.

If we have multiple detectors of number N, the observational time T can be effectively increased to $T \times N(N-1)/2$ by correlating all pairs of data from N detectors. Figure 7 shows sensitivity behaviors of multiple SOGROs and aSOGROs for the power-law model parameter

Downloaded from https://academic.oup.com/ptep/article/2024/5/053E01/7639407 by Ewha Womans University user on 31 October 2024

$\alpha = 0$. Orange and blue dots represent the networks consisting of N SOGROs and N aSOGROs, respectively. The horizontal solid line shows the level of indirect limits given in Fig. 6 for the power-law model parameter $\alpha = 0$. Although about 47 SOGRO detectors are required for the equivalent performance of a two-aSOGRO network, a relatively small number (about 6) of SOGRO detectors can touch the indirect limit.

5. Discussion

We have investigated the characteristics of the SOGRO detector concepts that can observe GWs in 0.1–10 Hz and the plausible science cases with those. We consider two different concepts labeled as SOGRO and aSOGRO depending on the size and their specification. Based on the detector characteristics, we obtain response functions for all detection channels of a SOGRO detector, given GW polarizations including even vector, scalar, breathing, and longitudinal modes which may appear in alternative gravity theories. By combining responses from all channels, we conclude that SOGRO is essentially an omnidirectional GW detector. Furthermore, the tensorial nature of the SOGRO data makes it possible to localize the source position from observation with a single detector.

SOGRO and aSOGRO with the expected sensitivities can detect IMBHs with the total mass range of about $(10^2$–$10^5)$ $M_\odot$. aSOGRO can reach up to ∼6.7 Gpc for IMBHs with about $(1.5 \times 10^4$–$1.5 \times 10^4)$ $M_\odot$ BBHs. This implies a detection rate of (3.1–8.1) IMBHBs per year in the most optimistic case. For the stellar-mass BHs, the GW signals can remain in SOGRO's frequency band for days to months, which will help to estimate parameters more accurately. Additionally, it can be a precursor to LVK observations due to its lower frequency band. For the SGWBs, a SOGRO detector network would allow us to constrain different models of the SGWB such as the cosmological indirect limits if multiple detectors based on the SOGRO or aSOGRO design are to be realized.

There are many technical challenges in the development of SOGRO detectors. They include Newtonian noise mitigation, highly-sensitive SQUID sensor development, civil engineering of large platforms underground, analyzing the bending effect of long arms, etc. It was shown in Ref. [19] that Newtonian noises originated from seismic and atmospheric density fluctuations can greatly be mitigated by optimally combining SOGRO channels with a modest number of seismometers and microphones. However, the subtraction of infrasound noise still does not reach the required sensitivity limit. In addition, the finite size effect of the SOGRO detector might be taken into account for more accurate modeling as mentioned in Ref. [19]. A dedicated work to tackle the issue of Newtonian noise mitigation is strongly called for. In particular, the Newtonian noise mitigation requires a deep underground construction at a scale larger than $(50 \times 50 \times 50)$ m^3.

The SOGRO or aSOGRO platform including six TMs weighs around 250 tons. According to the proposed design, the weight should be suspended by a single string or multiple strings at the center to form a pendulum as a whole. This requires that any vibrational noise produce only common motions of the ideal rigid platform through the suspension. An optimal platform design satisfying various requirements has been suggested in Ref. [14]. However, we note that practical civil engineering issues about how to construct and suspend the platform should further be investigated.

Downloaded from https://academic.oup.com/ptep/article/2024/5/053E01/7639407 by Ewha Womans University user on 31 October 2024

Funding

This research was partially supported by the National Research Council of Science & Technology (NST) grant by the Korean government (MSIP) (No. PCS-17-06-KASI). C.K. was partially supported by the National Research Foundation of Korea (NRF) grant NRF-2021R1F1A1062969 and the Ewha Womans University Research Grant of 2023. C.P. and Y.-B.B. were supported in part by Institute for Basic Science (IBS) under Project Code No. IBS-R018-D1. C.P. would also like to acknowledge Asia Pacific Center for Theoretical Physics (APCTP) for the supports through its activity programs. Y.-B.B., E.J.S., and H.M.L. were supported by NRF grants No. NRF-2021R1F1A1051269, No. 2021R1A2C1093059, and No. 2021M3F7A1082056 funded by the Korean government (MSIT), respectively. C.P., J.J.O., and G.K. were supported in part by the Basic Science Research Program through the NRF funded by the Ministry of Education with grant numbers NRF-2018R1D1A1B07041004, NRF-2020R1I1A2054376, and 2022R1I1A207366012, respectively. G.K. is supported in part by NRF grant No. NRF-2021R1A2C201247313. H.J.P. and R.S.N. acknowledge the support from the National Science Foundation through grant numbers PHY-1912627 and PHY-2207757.

Acknowledgements

The authors would like to acknowledge Korea Astronomy and Space Science Institute (KASI), Korea Institute of Science and Technology Information (KISTI), and National Institute for Mathematical Sciences (NIMS) for their various supports when this work was initiated.

Appendix. Response functions for extra polarizations of GWs

Alternative theories of gravity could allow extra polarization degrees of freedom for GWs in addition to the plus and cross ones in general relativity. Here, the response functions for such extra modes are summarized for the laser interferometer and SOGRO detectors. First of all, the three unit vectors mentioned in Sect. 3.1 are explicitly given by

$$\begin{aligned}
\hat{u} &= (\sin\phi\cos\psi + \cos\theta\cos\phi\sin\psi, -\cos\phi\cos\psi + \cos\theta\sin\phi\sin\psi, -\sin\theta\sin\psi),\\
\hat{v} &= (\cos\theta\cos\phi\cos\psi - \sin\phi\sin\psi, \cos\theta\sin\phi\cos\psi + \cos\phi\sin\psi, -\sin\theta\cos\psi),\\
\hat{n} &= (\sin\theta\cos\phi, \sin\theta\sin\phi, \cos\theta),
\end{aligned} \tag{A1}$$

where θ and ϕ are the polar and azimuthal angles of the propagating direction $\hat{n}$, respectively, and ψ is the polarization angle.

For the laser interferometer, the response functions for GWs having vector, breathing, and longitudinal polarizations are given by

$$\begin{aligned}
\mathrm{F}_x(\theta,\phi,\psi) &= \sin\theta\sin 2\phi\cos\psi + \frac{1}{2}\sin 2\theta\cos 2\phi\sin\psi,\\
\mathrm{F}_y(\theta,\phi,\psi) &= \frac{1}{2}\sin 2\theta\cos 2\phi\cos\psi - \sin\theta\sin 2\phi\sin\psi,\\
\mathrm{F}_b(\theta,\phi,\psi) &= -\frac{1}{2}\sin^2\theta\cos 2\phi,\\
\mathrm{F}_l(\theta,\phi,\psi) &= \frac{1}{\sqrt{2}}\sin^2\theta\cos 2\phi,
\end{aligned} \tag{A2}$$

Downloaded from https://academic.oup.com/ptep/article/2024/5/053E01/7639407 by Ewha Womans University user on 31 October 2024

respectively. For SOGRO channels, on the other hand, they become

$$
\begin{aligned}
\mathrm{F}_x^{(11)} &= \sin\theta \sin 2\phi \cos\psi + \sin 2\theta \cos^2\phi \sin\psi, \\
\mathrm{F}_x^{(22)} &= -\sin\theta \sin 2\phi \cos\psi + \sin 2\theta \sin^2\phi \sin\psi, \\
\mathrm{F}_x^{(12)} &= -\sin\theta \cos 2\phi \cos\psi + \frac{1}{2}\sin 2\theta \sin 2\phi \sin\psi, \\
\mathrm{F}_y^{(11)} &= -\sin\theta \sin 2\phi \sin\psi + \sin 2\theta \cos^2\phi \cos\psi, \\
\mathrm{F}_y^{(22)} &= \sin 2\theta \sin^2\phi \cos\psi + \sin\theta \sin 2\phi \sin\psi, \\
\mathrm{F}_y^{(12)} &= \frac{1}{2}\sin 2\theta \sin 2\phi \cos\psi + \sin\theta \cos 2\phi \sin\psi, \\
\mathrm{F}_b^{(11)} &= \sin^2\phi + \cos^2\theta \cos^2\phi, \quad \mathrm{F}_b^{(12)} = -\frac{1}{2}\sin^2\theta \sin 2\phi, \\
\mathrm{F}_l^{(11)} &= \sqrt{2}\sin^2\theta \cos^2\phi, \quad \mathrm{F}_l^{(12)} = \frac{1}{\sqrt{2}}\sin^2\theta \sin 2\phi,
\end{aligned}
\tag{A3}
$$

respectively. Response functions of a SOGRO detector were defined in Eq. (11).

References

[1] B. P. Abbott et al. [LIGO Scientific Collaboration, Virgo Collaboration], Phys. Rev. Lett. **116**, 061102 (2016) [arXiv:1602.03837[gr-qc]] [Search inSPIRE].
[2] J. Aasi et al. [LIGO Scientific Collaboration], Class. Quant. Grav. **32**, 074001 (2015) [arXiv:1411.4547[gr-qc]] [Search inSPIRE].
[3] F. Acernese et al., Class. Quant. Grav. **32**, 024001 (2015) [arXiv:1408.3978[gr-qc]] [Search inSPIRE].
[4] T. Akutsu et al. [KAGRA Collaboration], Nat. Astron. **3**, 35 (2019) [arXiv:1811.08079[gr-qc]] [Search inSPIRE].
[5] J. Antoniadis et al., Astron. Astrophys. **678**, A50 (2023) [arXiv:2306.16214[astro-ph.HE]] [Search inSPIRE].
[6] J. Antoniadis et al., The second data release from the European Pulsar Timing Array IV. Search for continuous gravitational wave signals, (June 2023) [arXiv:2306.16226[astro-ph]] [Search inSPIRE].
[7] D. J. Reardon et al., Astrophys. J. Lett. **951**, L6 (2023) [arXiv:2306.16215[astro-ph.HE]] [Search in SPIRE].
[8] G. Agazie et al., Astrophys. J. Lett. **951**, L8 (2023) [arXiv:2306.16213[astro-ph.HE]] [Search inSPIRE].
[9] H. Xu et al., Res. Astron. Astrophys. **23**, 075024 (2023) [arXiv:2306.16216[astro-ph.HE]] [Search inSPIRE].
[10] P. Amaro-Seoane et al., Laser Interferometer Space Antenna, (February 2017), [arXiv:1702.00786[astro-ph]] [Search inSPIRE]
[11] M. Punturo et al., Class. Quant. Grav. **27**, 194002 (2010).
[12] J. Harms, B. J. J. Slagmolen, R. X. Adhikari, M. Coleman, M. Evans, Y. Chen, H. Müller, and M. Ando, Phys. Rev. D **88**, 122003 (2013).
[13] H. J. Paik, C. E. Griggs, M. Vol Moody, K. Venkateswara, H. M. Lee, A. B. Nielsen, E. Majorana, and J. Harms, Class. Quant. Grav. **33**, 075003 (2016).
[14] H. J. Paik, M. Vol Moody, and R. S. Norton, Int. J. Mod. Phys. D **29**, 1940001 (2020).
[15] S. Kawamura et al., Prog. Theor. Exp. Phys. **2021**, 05A105 (2021) [arXiv:2006.13545[gr-qc]] [Search inSPIRE].
[16] M. Ando, K. Ishidoshiro, K. Yamamoto, K. Yagi, W. Kokuyama, K. Tsubono, and A. Takamori, Phys. Rev. Lett. **105**, 161101 (2010).
[17] B. Canuel et al., Sci. Rep. **8**, 14064 (2018) [arXiv:1703.02490[physics.atom-ph]] [Search inSPIRE].
[18] J. Crowder and N. J. Cornish, Phys. Rev. D **72**, 083005 (2005) [arXiv:gr-qc/0506015] [Search inSPIRE].
[19] J. Harms and H. J. Paik, Phys. Rev. D **92**, 022001 (2015).

Downloaded from https://academic.oup.com/ptep/article/2024/5/053E01/7639407 by Ewha Womans University user on 31 October 2024

[20] R. V. Wagoner, C. M. Will, and H. J. Paik, Phys. Rev. D **19**, 2325 (1979).
[21] H. J. Paik, Sensitivity and bandwidth of resonant-mass gravitational wave detectors.In: S.-W. Kim, editor. Proceedings of the International Workshop on Gravitation and Fifth Force, December 20-21, 1993 (Kyung Moon Sa, Seoul, 1993), p. 1.
[22] H. J. Paik, Nuovo Cim. B **55**, 15 (1980).
[23] H. J. Paik, Phys. Rev. D **33**, 309 (1986).
[24] H. A. Chan and H. J. Paik, Phys. Rev. D **35**, 3551 (1987).
[25] H. A. Chan, M. V. Moody, and H. J. Paik, Phys. Rev. D **35**, 3572 (1987).
[26] M. Vol Moody, H. J. Paik, and E. R. Canavan, Rev. Sci. Instrum. **73**, 3957 (2002).
[27] H. J. Paik, EPJ Web Conf. **168**, 01005 (2018).
[28] C. Cinquegrana, P. Rapagnani, F. Ricci, and E. Majorana, Phys. Rev. D **48**, 448 (1993).
[29] H. J. Paik, Phys. Rev. D **15**, 409 (1977).
[30] W. W. Johnson and S. M. Merkowitz, Phys. Rev. Lett. **70**, 2367 (1993).
[31] Mini-GRAIL (Gravitational Radiation Antenna In Leiden), Homepage: http://www.minigrail.nl/.
[32] K. Eda, A. Shoda, Y. Itoh, and M. Ando, Phys. Rev. D **90**, 064039 (2014) [arXiv:1406.7059[gr-qc]] [Search inSPIRE].
[33] A. Nishizawa, A. Taruya, K. Hayama, S. Kawamura, and M.-a. Sakagami, Phys. Rev. D **79**, 082002 (2009) [arXiv:0903.0528[astro-ph.CO]] [Search inSPIRE].
[34] N. Christensen, Phys. Rev. D **46**, 5250 (1992).
[35] B. S. Sathyaprakash and B. F. Schutz, Living Rev. Rel. **12**, 2 (2009) [arXiv:0903.0338[gr-qc]] [Search inSPIRE].
[36] V. Varma, P. Ajith, S. Husa, J. C. Bustillo, M. Hannam, and M. Puerrer, Phys. Rev. D **90**, 124004 (2014) [arXiv:1409.2349[gr-qc]] [Search inSPIRE].
[37] Y.-H. Hyun, Y. Kim, and S. Lee, Phys. Rev. D **99**, 124002 (2019) [arXiv:1810.09316[gr-qc]] [Search inSPIRE].
[38] L. S. Finn, Phys. Rev. D **63**, 102001 (2001) [arXiv:gr-qc/0010033] [Search inSPIRE].
[39] B. P. Abbott et al. [LVK Collaboration], Living Rev. Rel. **23**, 3 (2020).
[40] C. Z. Zhou and P. F. Michelson, Phys. Rev. D **51**, 2517 (1995).
[41] B. Allen and J. D. Romano, Phys. Rev. D **59**, 102001 (1999) [arXiv:gr-qc/9710117] [Search inSPIRE].
[42] B. P. Abbott et al. [LIGO Scientific Collaboration, Virgo Collaboration], Phys. Rev. X **9**, 031040 (2019) [arXiv:1811.12907[astro-ph.HE]] [Search inSPIRE].
[43] R. Abbott et al. [LIGO Scientific Collaboration, Virgo Collaboration], Phys. Rev. X **11**, 021053 (2021) [arXiv:2010.14527[gr-qc]] [Search inSPIRE].
[44] R. Abbott et al. [LIGO Scientific Collaboration, Virgo Collaboration], Phys. Rev. D **109**, 022001 (2024) [arXiv:2108.01045[gr-qc]] [Search inSPIRE].
[45] R. Abbott et al. [LVK Collaboration], Phys. Rev. X **13**, 041039 (2023) [arXiv:2111.03606[gr-qc]] [Search inSPIRE].
[46] J. Abadie et al., Class. Quant. Grav. **27**, 173001 (2010) [arXiv:1003.2480[astro-ph.HE]] [Search inSPIRE].
[47] D. Merritt, Black holes and galaxy evolution. In: F. Combes, G. A. Mamon, and V. Charmandaris, editors. Dynamics of galaxies: from the early universe to the present, Astronomical Society of the Pacific Conference Series, vol. **197**(Astronomical Society of the Pacific, San Francisco, 2000). p. 221[arXiv:astro-ph/9910546] [Search inSPIRE].
[48] L. Ferrarese and D. Merritt, Astrophys. J. Lett. **539**, L9 (2000) [arXiv:astro-ph/0006053] [Search inSPIRE].
[49] K. Gebhardt et al., Astrophys. J. Lett. **539**, L13 (2000) [arXiv:astro-ph/0006289] [Search inSPIRE].
[50] N. J. McConnell, C.-P. Ma, K. Gebhardt, S. A. Wright, J. D. Murphy, T. R. Lauer, J. R. Graham, and D. O. Richstone, Nature **480**, 215 (2011) [arXiv:1112.1078[astro-ph.CO]] [Search inSPIRE].
[51] J. Kormendy and L. C. Ho, Annu. Rev. Astron. Astrophys. **51**, 511 (2013) [arXiv:1304.7762[astro-ph.CO]] [Search inSPIRE].
[52] A. Patruno, S. Portegies Zwart, J. Dewi, and C. Hopman, Mon. Not. R. Astron. Soc. **370**, L6 (2006) [arXiv:astro-ph/0602230] [Search inSPIRE].
[53] T. J. Maccarone, A. Kundu, S. E. Zepf, and K. L. Rhode, Nature **445**, 183 (2007) [arXiv:astro-ph/0701310] [Search inSPIRE].

Downloaded from https://academic.oup.com/ptep/article/2024/5/053E01/7639407 by Ewha Womans University user on 31 October 2024

[54] I. V. Chilingarian, I. Y. Katkov, I. Y. Zolotukhin, K. A. Grishin, Y. Beletsky, K. Boutsia, and D. J. Osip, Astrophys. J. **863**, 1 (2018) [arXiv:1805.01467[astro-ph.GA]] [Search inSPIRE].
[55] S. Takekawa, T. Oka, Y. Iwata, S. Tsujimoto, and M. Nomura, Astrophys. J. Lett. **871**, L1 (2019) [arXiv:1812.10733[astro-ph.GA]] [Search inSPIRE].
[56] J.-H. Woo, H. Cho, E. Gallo, E. Hodges-Kluck, H. A. N. Le, J. Shin, D. Son, and J. C. Horst, Nat. Astron. **3**, 755 (2019) [arXiv:1905.00145[astro-ph.GA]] [Search inSPIRE].
[57] J. E. Greene, J. Strader, and L. C. Ho, Annu. Rev. Astron. Astrophys. **58**, 257 (2020) [arXiv:1911.09678[astro-ph.GA]] [Search inSPIRE].
[58] P. Ajith et al., Phys. Rev. Lett. **106**, 241101 (2011) [arXiv:0909.2867[gr-qc]] [Search inSPIRE].
[59] P. A. R. Ade et al., Astron. Astrophys. **594**, A13 (2016) [arXiv:1502.01589[astro-ph.CO]] [Search inSPIRE].
[60] M. Giersz, N. Leigh, A. Hypki, A. Askar, and N. Lützgendorf, Mem. Soc. Astron. Ital. **87**, 555 (2016) [arXiv:1607.08384[astro-ph.GA]] [Search inSPIRE].
[61] J. M. Fregeau, S. L. Larson, M. C. Miller, R. O'Shaughnessy, and F. A. Rasio, Astrophys. J. Lett. **646**, L135 (2006) [arXiv:astro-ph/0605732] [Search inSPIRE].
[62] P. Amaro-Seoane and L. Santamaría, Astrophys. J. **722**, 1197 (2010) [arXiv:0910.0254[astro-ph.CO]] [Search inSPIRE].
[63] S. F. Portegies Zwart, J. Makino, S. L. W. McMillan, and P. Hut, Astron. Astrophys. **348**, 117 (1999) [arXiv:astro-ph/9812006] [Search inSPIRE].
[64] T. Ebisuzaki, J. Makino, T. G. Tsuru, Y. Funato, S. Portegies Zwart, P. Hut, S. McMillan, S. Matsushita, H. Matsumoto, and R. Kawabe, Astrophys. J. Lett. **562**, L19 (2001) [arXiv:astro-ph/0106252] [Search inSPIRE].
[65] S. F. Portegies Zwart and S. L. W. McMillan, Astrophys. J. **576**, 899 (2002) [arXiv:astro-ph/0201055] [Search inSPIRE].
[66] S. F. Portegies Zwart, H. Baumgardt, P. Hut, J. Makino, and S. L. W. McMillan, Nature **428**, 724 (2004) [arXiv:astro-ph/0402622] [Search inSPIRE].
[67] M. A. Gürkan, M. Freitag, and F. A. Rasio, Astrophys. J. **604**, 632 (2004) [arXiv:astro-ph/0308449] [Search inSPIRE].
[68] P. Madau and L. Pozzetti, Mon. Not. R. Astron. Soc. **312**, L9 (2000) [arXiv:astro-ph/9907315] [Search inSPIRE].
[69] C. C. Steidel, K. L. Adelberger, M. Giavalisco, M. Dickinson, and M. Pettini, Astrophys. J. **519**, 1 (1999) [arXiv:astro-ph/9811399] [Search inSPIRE].
[70] A. W. Blain, J. P. Kneib, R. J. Ivison, and I. Smail, Astrophys. J. Lett. **512**, L87 (1999) [arXiv:astro-ph/9812412] [Search inSPIRE].
[71] C. Porciani and P. Madau, Astrophys. J. **548**, 522 (2001) [arXiv:astro-ph/0008294] [Search inSPIRE].
[72] D. E. McLaughlin, Astron. J. **117**, 2398 (1999) [arXiv:astro-ph/9901283] [Search inSPIRE].
[73] M. Freitag, F. A. Rasio, and H. Baumgardt, Mon. Not. R. Astron. Soc. **368**, 121 (2006) [arXiv:astro-ph/0503129] [Search inSPIRE].
[74] M. Freitag, M. A. Gürkan, and F. A. Rasio, Mon. Not. R. Astron. Soc. **368**, 141 (2006) [arXiv:astro-ph/0503130] [Search inSPIRE].
[75] Q. Zhang and S. M. Fall, Astrophys. J. Lett. **527**, L81 (1999) [arXiv:astro-ph/9911229] [Search inSPIRE].
[76] P. Amaro-Seoane and M. Freitag, Astrophys. J. Lett. **653**, L53 (2006) [arXiv:astro-ph/0610478] [Search inSPIRE].
[77] M. Arca Sedda et al., Class. Quant. Grav. **37**, 215011 (2020) [arXiv:1908.11375[gr-qc]] [Search inSPIRE].
[78] D. Gerosa and E. Berti, Phys. Rev. D **95**, 124046 (2017) [arXiv:1703.06223[gr-qc]] [Search inSPIRE].
[79] H. Shinkai, N. Kanda, and T. Ebisuzaki, Astrophys. J. **835**, 276 (2017) [arXiv:1610.09505[astro-ph.GA]] [Search inSPIRE].
[80] T. Nakamura et al., Prog. Theor. Exp. Phys. **2016**, 093E01 (2016) [arXiv:1607.00897[astro-ph.HE]] [Search inSPIRE].
[81] R. Abbott et al. [LVK Collaboration], Phys. Rev. X **13**, 011048 (2023) [arXiv:2111.03634[astro-ph.HE]] [Search inSPIRE].

Downloaded from https://academic.oup.com/ptep/article/2024/5/053E01/7639407 by Ewha Womans University user on 31 October 2024

[82] B. Carr and F. Kühnel, Annu. Rev. Nucl. Part. Sci. **70**, 355 (2020) [arXiv:2006.02838[astro-ph.CO]] [Search inSPIRE].
[83] S. Shandera, D. Jeong, and H. S. Grasshorn Gebhardt, Phys. Rev. Lett. **120**, 241102 (2018) [arXiv:1802.08206[astro-ph.CO]] [Search inSPIRE].
[84] A. H. Nitz and Y.-F. Wang, Phys. Rev. Lett. **127**, 151101 (2021) [arXiv:2106.08979[astro-ph.HE]] [Search inSPIRE].
[85] E. Thrane and J. D. Romano, Phys. Rev. D **88**, 124032 (2013).
[86] V. Mandic and E. Floden, An interactive plotter for energy spectrum of stochastic gravitational wave backgrounds from various theoretical models, https://groups.spa.umn.edu/gwplotter/.
[87] R. Abbott et al. [LVK Collaboration], Phys. Rev. D **104**, 022004 (2021).
[88] P. D. Lasky et al., Phys. Rev. X **6**, 011035 (2016).
[89] N. Cornish and T. Robson, J. Phys. Conf. Ser. **840**, 012024 (2017).
[90] Y. Akrami et al., Astron. Astrophys. **641**, A10 (2020).

Downloaded from https://academic.oup.com/ptep/article/2024/5/053E01/7639407 by Ewha Womans University user on 31 October 2024

© The Author(s) 2024. Published by Oxford University Press on behalf of the Physical Society of Japan. This is an Open Access article distributed under the terms of the Creative Commons Attribution License (https://creativecommons.org/licenses/by/4.0/), which permits unrestricted reuse, distribution, and reproduction in any medium, provided the original work is properly cited.